

Rochester Institute of Technology

RIT Digital Institutional Repository

Theses

5-16-2013

An Investigation of electrochemomechanical actuation of conductive polyacrylonitrile (PAN) nanofiber composites

Mark Gonzalez

Follow this and additional works at: <https://repository.rit.edu/theses>

Recommended Citation

Gonzalez, Mark, "An Investigation of electrochemomechanical actuation of conductive polyacrylonitrile (PAN) nanofiber composites" (2013). Thesis. Rochester Institute of Technology. Accessed from

This Thesis is brought to you for free and open access by the RIT Libraries. For more information, please contact repository@rit.edu.

**An Investigation of Electrochemomechanical Actuation
of Conductive Polyacrylonitrile (PAN) Nanofiber Composites**

By:
Mark A. Gonzalez

A Thesis Submitted in Partial
Fulfillment of the Requirements for the

**MASTERS OF SCIENCE
IN
MECHANICAL ENGINEERING**

Approved: May 16, 2013

**DEPARTMENT OF MECHANICAL ENGINEERING
KATE GLEASON COLLEGE OF ENGINEERING
ROCHESTER INSTITUTE OF TECHNOLOGY**

Committee Signature Page

Approved By:

Dr. Wayne Walter
Professor, Thesis Advisor
Department of Mechanical Engineering

Signature: _____

Dr. Kathleen Lamkin-Kennard
Assistant Professor
Department of Mechanical Engineering

Signature: _____

Dr. Hany Ghoneim
Professor
Department of Mechanical Engineering

Signature: _____

Dr. Christiaan Richter
Assistant Professor
Department of Chemical Engineering

Signature: _____

Dr. Agamemnon Crassidis
Associate Professor, Dept. Representative
Department of Mechanical Engineering

Signature: _____

**DEPARTMENT OF MECHANICAL ENGINEERING
KATE GLEASON COLLEGE OF ENGINEERING
ROCHESTER INSTITUTE OF TECHNOLOGY**

May 16, 2013

Table of Contents

| | |
|--|-----|
| Title Page | |
| Signature Page | |
| Table of Contents..... | i |
| Abstract..... | iii |
| Acknowledgements..... | iv |
| List of Terms..... | v |
| | |
| Chapter 1: Introduction..... | 1 |
| 1.1 Skeletal Muscle Functions and Mechanisms | 2 |
| 1.2 Smart Materials for Actuation | 5 |
| 1.2.1 Dielectric Elastomers (DEAPs)..... | 5 |
| 1.2.2 Ionic Polymer/Metal Composites (IPMCs) | 7 |
| 1.2.3 Shape Memory Alloys (SMAs)..... | 8 |
| 1.2.4 Intrinsically Conductive Polymers (ICPs)..... | 8 |
| 1.3 Biomimetic Analysis of Skeletal Muscles..... | 10 |
| | |
| Chapter 2: PAN Material Properties, Processing, and Performance..... | 12 |
| 2.1 Properties of Polyacrylonitrile..... | 12 |
| 2.2 PAN Activation Processing..... | 13 |
| 2.3 Actuation Performance of PAN Fibers..... | 14 |
| 2.4 Electrospinning..... | 17 |
| 2.5 Parameter Effects on Electrospinning..... | 19 |
| 2.5.1 Concentration..... | 19 |
| 2.5.2 Collection Distance | 21 |
| 2.5.3 Dielectric Solvent..... | 22 |
| 2.5.4 Humidity..... | 23 |
| 2.6 Actuation Performance of PAN Nanofibers | 23 |
| | |
| Chapter 3: Chemical and Electro-chemical Actuation Mechanism | 24 |
| 3.1 Activated PAN Fibers..... | 24 |
| 3.2 Chemical Actuation..... | 25 |
| 3.3 Electro-chemical Actuation: Electrolysis..... | 27 |

| | |
|---|----|
| 3.4 Improving PAN Fiber Conductivity | 29 |
| 3.5 Activating Conductive PAN Nanofiber Composites for Actuation (Aims of Research)..... | 31 |
| Chapter 4: Experimental Procedures and Results..... | 33 |
| 4.1 PAN Nanofiber Fabrication..... | 33 |
| 4.2 Chemical Activation | 35 |
| 4.3 Electrochemical Actuation | 36 |
| 4.4 Introduction of Conductive Additive to Electrospinning | 38 |
| 4.5 Alternative Conductive Electrode Materials..... | 41 |
| 4.6 Transient Variation of Localized pH..... | 43 |
| 4.7 Processed PAN Nanofiber Tensile Testing | 45 |
| 4.8 PAN/Graphite Composite Actuator (Prototype I) | 53 |
| 4.9 Modifications to PAN/Graphite Composite Design (Prototype II)..... | 55 |
| Chapter 5: Discussion of Results..... | 57 |
| 5.1 Conductive Additives..... | 57 |
| 5.2 Alternative Electrode Materials..... | 58 |
| 5.3 PAN Nanofiber Mat Properties | 59 |
| Chapter 6: Conclusion..... | 61 |
| Chapter 7: Future Work..... | 63 |
| References... .. | 64 |
| Appendix A: Summary of Current Actuator Properties..... | 69 |
| Appendix B: Characteristics and Challenges of Dielectric Elastomers..... | 70 |
| Appendix C: Tensile Testing Data..... | 71 |
| Appendix D: Panasonic “PGS” Graphite Sheets..... | 77 |
| Appendix E: Sylgard 184 Silicone Elastomer..... | 81 |
| Appendix F: Drawing of Graphite Spring Electrode..... | 84 |

Abstract

A polymer-based nanofiber composite actuator designed for linear actuation was fabricated by electrospinning, actuated by electrolysis, and characterized by electrical and mechanical testing to address performance limitations and understand the activation processing effects on actuation performance. Currently, Electroactive polymers (EAPs) have provided uses in sensory and actuation technology, but have either low force output or expand rather than contract, falling short in capturing the natural motion and function of muscle desperately needed to provide breakthroughs in the bio-medical and robotic fields. Previous research has shown activated Polyacrylonitrile (PAN) fibers having biomimetic functionalities similar to the sarcomere contraction responsible for muscle function. Activated PAN is also known to contract and expand by electrolysis when in close vicinity to the anode and cathode, respectively. PAN nanofibers especially show faster response to changes in environmental pH and improved mechanical properties over larger diameter fibers. Conductive additives were introduced to the electrospinning solution and activated in an attempt to create composite PAN nanofiber gel actuators with improved conductivity and eliminate the need of stiff electrodes. Tensile testing was conducted to examine changes in mechanical properties between annealing and hydrolysis processing. Introducing conductive additives did not show a significant increase in conductivity and created unusable samples, requiring alternative electrode materials. Electrochemical contraction rates up to 25%/min were achieved. Strains of 58.8%, ultimate stresses up to 77.1 MPa, and moduli of 0.21 MPa were achieved with pure PAN nanofiber mats, surpassing mechanical properties of natural muscles. Improvements to contraction rates and young's moduli are necessary to capture the function and performance of skeletal muscles properly.

Acknowledgements

First of all, I want to thank my advisor, Dr. Wayne Walter, for giving me the opportunity to pursue this field of research I've been interested in long before entering RIT. I would like to thank my committee members Dr. Kathleen Lamkin-Kennard, Dr. Hany Ghoneim, and Dr. Christaan Richter for providing their support and encouragement throughout the way. I would also like to Thank Dr. Hans Schmitthenner, Dr. Scott Williams, Tom Grimsley, Dave Hathaway, and Dr. Surendra Gupta for providing me the necessary equipment, resources, and lab space. Furthermore, I would like to thank William Spath and Harry Singh for all the help along the way. Lastly, I would like to thank my parents, because even though they may never fully understand what I do or why I do it, they will always support me knowing this is what I am most passionate about. And for that, I am eternally grateful.

List of Terms

Adenosine Triphosphate (ATP) – a molecule typically found in living organisms, capable of providing energy for cell division, material transport, muscle contraction, and other cellular activities.

Amphoteric – a chemical property of a molecule or ion to donate or accept protons, reacting as either an acid or base, respectively.

Aromatization Index (AI) – A numeric value used to determine the percentage of molecular ring structures present within a given sample using wide-angle X-ray diffraction.

Dielectric Elastomer – A compliant capacitor that produces large strains using electrostatic pressures. A type of Electroactive polymer.

Electroactive Polymer – A polymeric material that is stimulated by an electric field, causing volumetric deformations to the material.

Isometric testing – An actuation test characterizing the contractile forces generated from an actuator held at a static displacement

Isotonic testing – An actuation test characterizing the maximum displacement achieved from an actuator with a constant force applied in a resistive manner.

Chapter 1: Introduction

The foundation of this research, to develop a PAN-based actuator, has strongly been supported by the concept of biomimetics. Biomimetics is the study of a biological system's structure and function to act as a source of inspiration for design concepts and engineering solutions [1]. Nature, through evolution and adaptation, has managed to create complex biological systems within flora and fauna over millions of years. The successes of this natural trial and error process are showcased throughout all biological creatures and various natural phenomena. Basing our inspiration on such successful natural “experiments” would serve as a proper starting point for new technological advances and understanding.

We have been borrowing ideas from nature for hundreds of years. Leonardo da Vinci studied birds and how they achieved flight. As a result, he developed the Ornithopter as an attempt to fly like birds (See Figure 1) [2]. In a more recent era, Speedo, a swimwear manufacturer, developed swimsuits utilizing the varying textures of shark skin as inspiration to reduce drag and control flow on a swimmer [3]. Another example is the lotus flower and its ability to repel water. The lotus’s unique coating has inspired the design of super hydrophobic surfaces for self-cleaning materials [4]. As many innovations have stemmed from nature’s design, mimicking the human body and the various functions is an ongoing challenge worthy of exploration.

With advances in robotics, artificial intelligence, medicine, and cybernetics, the human race is approaching towards the development of artificial humans. For example, MIT researchers have developed a computer chip capable of mimicking the activity of a single brain synapse, providing insight into learning and memory production [5]. Development has also been made by the bioprinting company Organovo towards recreating tissue with the use of stem cells and 3D

printers [6]. As efforts are made towards understanding our brain and physiology, efforts towards understanding human locomotion and the mechanisms of muscles are equally important.



Figure 1: Leonardo da Vinci's plans for an Ornithopter, a flying machine kept aloft by the beating of its wings; about 1490 [2]

1.1 Skeletal Muscle Functions and Mechanisms

Skeletal muscles are soft tissue found within most animals providing a means of locomotion. These muscles are tethered to the skeletal system through tendons to create moments of force and provide rotational motion to limbs and digits. As the muscle contracts, a pulling force is generated and applied to the joint. It has been shown that isolated muscle fibers can contract upwards of $\pm 50\%$, although only $\pm 10\%$ contraction is observed for limb movement. [8] The interest in understanding the contraction mechanism as well as the associated mechanical properties brought forth histological investigations into skeletal muscle mechanics and functions with the hopes of mimicking such functions through artificial technology.

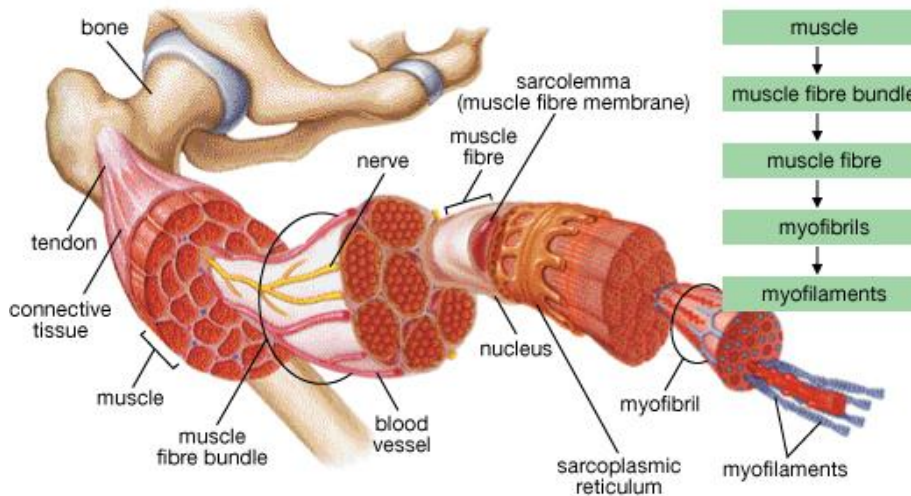


Figure 2: Structural Anatomy of the Human Muscle [9]

Skeletal muscles consist of multiple myocytes (muscle fibers) tethered together in a parallel configuration (See Figure 2). Muscle fibers typically have a diameter between 10 - 100 μm , dependent on genetics and level of strength. [10] Each muscle fiber consists of smaller myofibrils containing long chains of sarcomeres with diameters of 1-2 μm . The sarcomere is considered to be the basic unit of muscle made of actin (thin) and myosin (thick) myofilaments that supports muscle function. These myofilaments have been observed to maintain its original length and slide past one another, caused by cross bridges pulling on actin filaments and reducing the length of the sarcomere. This “sliding filament” mechanism shown in Figure 3, proposed by Hugh Huxley describes how sarcomeres shorten, translating to large scale muscle contraction [11].

The sarcomere contraction is initiated by the release of Ca^{+2} from the sarcoplasmic reticulum (SR) membrane surrounding the myofilaments. The SR membrane is responsible for the exposure and removal of Ca^{+2} to and from the myosin and actin filaments when triggered by motor neuron stimuli. As the concentration of Ca^{+2} increases, filament sliding begins and as the concentration decreases, the sliding ceases. The Ca^{+2} exposure coupled with the available high

energy molecule Adenosine triphosphate (ATP) necessary for cell metabolism provides the energy required to complete the contraction process [10].

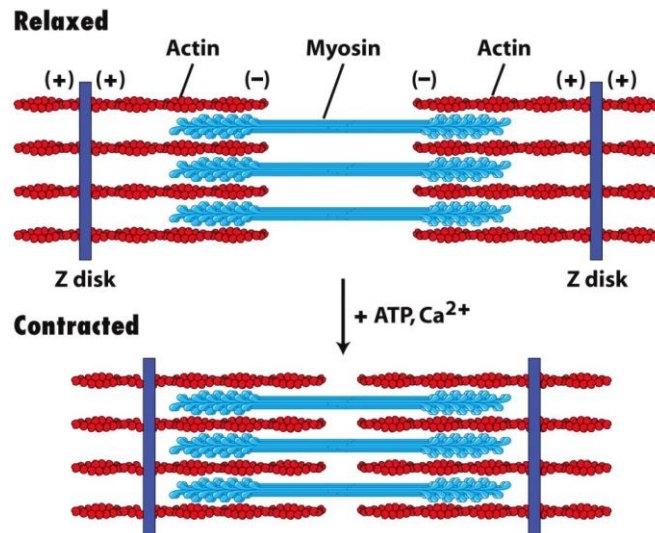


Figure 3: Relaxed and Contracted State of Sarcomere [12]

Muscles contain various properties desired for actuator technologies. Muscles have the ability to vary stiffness as the given situation requires. For example, catching a ball requires an arm stiff enough to stop the ball but soft enough to avoid receiving a large impulse on contact. The human body can adapt and optimize the stiffness of the incorporated muscles as needed. [13] Stiffness variance also contributes to the ability to gradually apply force through fiber recruitment, providing acceleration and force control. Table 1 lists additional properties of skeletal muscle in mammals.

Natural muscles can be recognized as the best existing actuator, not for a single dominating feature, but rather for its overall balanced performance and desired features [13, 14]. Various technologies have emphasized mimicking the essential function of muscles: linear contraction. Over time, the evolution of technology has driven actuator research into the

direction of biomimetics and began the exploration of alternatives using smart materials that closely mimic muscles.

Table 1: Mechanical Properties of Mammalian Skeletal Muscle [10]

| | |
|---------------------------------------|------------------|
| Maximum Strain (%) | >40 |
| Stress (MPa) | 0.35 |
| Density (kg·m⁻³) | 1037 |
| Strain Rate (%·s⁻¹) | >50 |
| Cycle Life | >10 ⁹ |
| Modulus (MPa) | 10 - 60 |

1.2: Smart Materials for Actuation

1.2.1: Dielectric Elastomers (DEAPs)

Dielectric elastomers are electroactive polymers that directly convert electrical energy into mechanical energy, and vice versa. Typically, two conductive layers sandwich a compliant elastomer film and through electrostatic attraction, the two layers compress the film. Large strains ranging from 10% upwards to 300% are achievable [13]. Although the compressive strain is high, volume must be conserved and a majority of the displacement expands the elastomer perpendicular to the compressive forces. Consequently, dielectrics are typically utilized in an expansive manner, contradictive to natural muscle's contraction-only function (See Figure 4).

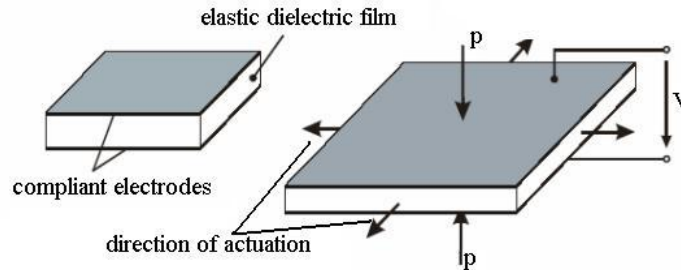


Figure 4: Dielectric Elastomer where V is applied voltage and p is the produced pressure [15]

Kovacs took advantage of the dielectric elastomer's compressive features and incorporated multiple DEAPs into a stack formation as shown in Figure 5. The benefit of an in-series stack allows the absolute deformation length to be dictated by the number of layers, simplifying the actuator design. [16]



Figure 5: DEAP Stack Actuator in passive mode (left) and active mode (right) [16]

Dielectric elastomers pose many limiting factors for actuation use. Dielectric breakdown is a significant failure mode that may result from imperfections in the thin polymer films as well as high strain rates [13, 17]. Typical dielectrics require high voltages to produce significant strain. Upwards to 150 MV/m is required, limiting the application for large and high frequency applications due to the energy requirements. Biddiss provides an extensive list of dielectric

actuator limitations including challenges in control, contaminant resistance, efficiency, and performance that can be found in Appendix A.

1.2.2: Ionic Polymer/Metal Composites (IPMCs)

Ionic Polymer/ Metal Composites are composed of a polymer electrolyte confined between two metal layers. By introducing an electric field, the ions located within the polymer will begin to polarize. Due to this polarization, the composite will begin to attract ions to one side of the polymer as well as water. The imbalance of water distribution causes swelling on one side and contraction on the other, causing the material to produce a bending motion. Factors such as thickness, surface area, type of polymer used, and amount and quality of water present all contribute to the amount of torque produced by the material.

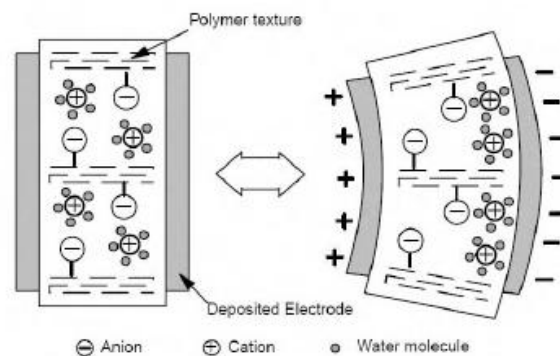


Figure 6: Ionic Polymer Metal Composite [18]

One apparent disadvantage of IPMCs is the generated torque. Muscles function in a linear manner whereas IPMCs provide bending actuation with very limited linear displacement. Incorporating IPMCs to impose linear displacements would require a novel design and orientation to produce linear actuation. Another limitation is the need to remain wet for operation. Maintaining hydration allows ions to diffuse across the material. Furthermore, due to

the electrical breakdown of water at 1.23 V, higher voltages degrade the displacement output of the IPMC [19].

1.2.3: Shape Memory Alloys (SMAs)

SMAs possess a unique ability to recover to its pre-deformed state with the application of heat. The material, typically Nitinol (NiTi), can be deformed and maintain its final orientation. By applying heat to the material bringing it beyond its transition temperature, the material returns to its original state, even after being cooled.

Due to the fact the metal alloys are actuated via joule heating, it is very difficult to control the displacement due to the ongoing phase transformations [13]. Also, since cooling due to free air convection is much slower than the heating phase, an active cooling method is required to match the heating and cooling times for symmetric actuation. SMAs do not have high tolerance to cyclic loading, limiting its long term use.

1.2.4: Intrinsically Conductive Polymers (ICPs)

Conductive polymers are organic structures featuring coupled structures supporting electron transport. These polymers can be actuated electrochemically. The electric charge along the polymer backbone can be increased or decreased through a change in oxidation state. The change in charge triggers a flow of ions towards or away from the polymer to restore the balance of electrical charge. Typically, a flow of ions into the polymer causes swelling and a flow of ions from the polymer reduces swelling, causing contraction (See Figure 7). Polypyrrole has been recognized as one of many suitable candidates for low voltage applications [21].

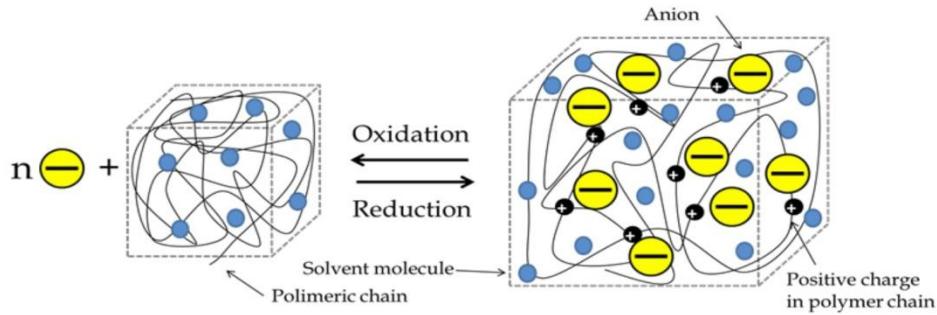


Figure 7: Swelling and Contraction of Conductive Polymer Chains. As positive charge is created in the polymer, negative ions (anions) flow into the polymer to restore charge balance. [20]

Conductive polymers have mechanical strengths much superior to natural muscles. Stresses up to 34 MPa can be supported with Moduli ranging from 0.1 to 3 GPa. The applied voltage required to actuate the material is low, ranging from 1.2 to 10 V. Low voltages would allow for portable devices such as prosthetics to operate without the need for large electrical equipment.

Although the required voltage is low in comparison to many other smart materials, high current is required to compensate for the very low electromechanical coupling in high power devices [21]. Overall strain and strain rates due to internal mechanical resistance limits the material's application towards fast actuators.

Table 2: Summary of natural muscle and various smart material properties. Adapted from [13]

| Property | Natural Muscle | Dielectric Elastomers | Ionic Polymer/Metal Composites | Shape Memory Alloys | Conductive Polymers |
|--------------------------------------|------------------|--|--------------------------------|-------------------------------|---------------------|
| Strain (%) | >40 | 380 | 3.3 | 8 | 12 |
| Strain Rate (%·s ⁻¹) | >50 | 4,500 | 3.3 | 300 | 12 |
| Stress (MPa) | 0.35 | 7.7 | 15 | 200 | 34 |
| Modulus (MPa) | 10-60 | 1.0 – 3.0 | 100 | 83,000 | 3,000 |
| Density (kg·m ⁻³) | 1,037 | 960 | 1,500 | 6,450 | - |
| Work Density (kJ·m ⁻³) | 40 | 3,400 | 5.5 | 10,000 | 1000 |
| Specific Power (W·kg ⁻¹) | 284 | 400 continuous 3,600 Peak | 2.56 | >50,000 | 150 |
| Cycle Life | >10 ⁹ | >10 ⁷ @ 5% strain 10 ⁶ @ 50% strain | - | 10 ⁷ @ 0.5% strain | 800,000 |

Of the mentioned smart materials, many show promise in sensory and other niche applications, but require additional development to be considered for flexible actuation applications. A summary of various smart material properties is provided in Table 2. One commonality amongst each candidate was either high force generation or high strain potential. Natural muscle possesses a dynamic balance of both properties to provide superior overall performance. Although researchers have been inspired by the linear contraction muscles produce, emphasis should be placed on understanding and incorporating the underlying biological operations supporting muscle function.

1.3: Biomimetic Analysis of Skeletal Muscles

Muscles operate through electrochemical and chemo-mechanical coupling. Electrical impulses from the spinal cord transfer to motor neurons signaling the release of Ca^{+2} and ATP use. The processing of Ca^{+2} and ATP initiates the filament sliding and the reactions can cycle at frequencies of 7 Hz and upwards, providing fast muscular motion [10]. Adopting these energy couplings provides a suitable configuration to transfer control signals to operate artificial muscle actuators.

Natural muscle contains an integrated circulatory system used to provide oxygen and energy to the surrounding muscular tissue as well as remove waste and heat. Various particles and heat are transferred across capillaries typically 10 μm in diameter [22]. Due to the density of capillaries within the tissue, the distances which particles and heat diffuse across are tens of micrometers. Emphasis must be made on taking advantage of the local delivery and removal for proper muscle function.

The benefits of locally exchanging resources and waste are a result of the scale of the myofilaments responsible for initiating actuation. Theoretically if the myofibrils were larger, limited diffusion rates would reduce the speed at which muscles can contract as well as the frequency of contraction. Thus, the micro and nanoscale dimensions of the myofibrils and myofilaments minimize diffusion issues. Thus, incorporating nanoscale features into a material may promote fast diffusion as well as benefit from the strength of materials at the nanoscale.

Although many of the potential smart materials perform well and possess similar properties as skeletal muscle, few show similar actuation mechanics. Our current understanding of sarcomeres and myofilaments grants us an attempt to mimic their functions one way or another. Polyacrylonitrile has shown promise as a candidate material and potentially capture many of the same functional features of sarcomeres [10].

Chapter 2: PAN Material Properties, Processing, and Performance

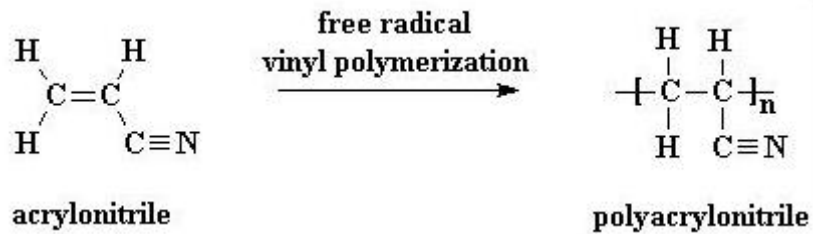


Figure 8: Synthesis of Polyacrylonitrile

2.1: Properties of Polyacrylonitrile

Polyacrylonitrile (PAN) is a synthetic organic polymer formed by the polymerization of acrylonitrile (AN). PAN is typically used in the textile industry for the production of artificial silk as well as outdoor fabrics [23]. The first woven fibers based on PAN were produced by the DuPont Corporation in 1941 under the trademark name Orlon [24]. Aside from textiles, PAN is used as a component for ABS plastic as well as a precursor for producing carbon fibers [25].

Although PAN is classified as a thermoplastic, it tends to degrade prior to melting. PAN's insolubility, thermal stability, and resistance to organic solvents make it a strong candidate as a biocompatible material. Due to comparable mechanical properties to natural muscle, in particular the large elongation and contraction percentages of activated PAN, development of artificial sarcomeres may be possible [26].

Bulk material properties of unprocessed PAN can be found in Table 3. Rosenbaum examined the mechanical behavior of macro scale PAN fibers. It was discovered that PAN fibers stretched upwards of 100% strain can recover to near 0% under the right kinetic conditions [27]. This high strain capability coupled with the tensile strength and similar density makes PAN fibers comparable to the mechanical properties of natural muscle. Before PAN fibers can be utilized as an artificial muscle actuator, it must be processed and activated.

Table 3: Bulk Mechanical Properties of Polyacrylonitrile [28]

| Elongation at Break (Yield) | Flexural Modulus | Tensile Strength | Young's Modulus | Density |
|-----------------------------|------------------|------------------|-----------------|----------------------------|
| 3-4% | 3.1-3.8 GPa | 50-65 MPa | 3.1-3.8 GPa | 1.1-1.15 g/cm ³ |

2.2: PAN Activation Processing

Figure 9 depicts the changes to the chemical structure of PAN made by pre-oxidation and hydrolysis. To improve the strength of the PAN fibers, the polymer is pre-oxidized. PAN prior to pre-oxidation, consists of individual molecular chains (See Figure 9a). Temperatures ranging between 220° to 300° C are exposed to the polymer, creating pyridine rings. These rings crosslink the polymers together, enhancing the elastomeric properties. The strength of the material is proportional to the amount of fiber crosslinking. Strong covalent bonds are formed between the PAN molecular chains within each fiber. As more and more crosslinks are formed, the deformed state of the material can provide stronger restorative forces and return to its undeformed state. This process can then be followed by a higher temperature carbonization process (~1000°C) to evolve the remaining nitrogen and oxygen to create high strength carbon fiber.

Pre-oxidized PAN contains pyridine rings as well as nitrile groups as shown in Figure 9b. The hydrolysis process, also known as saponification, converts the remaining nitrile groups to carboxyl acid groups (See Figure 9c). These groups are acknowledged as the driving mechanism for actuation [9]. Typically, inorganic hydroxides such as Sodium Hydroxide (NaOH) and Lithium Hydroxide (LiOH) are used to create the carboxyl acid groups. The hydroxide is heated to below boiling point (~ 95°C) and the annealed PAN fibers are introduced to the solution for 30 minutes. The 'activated' PAN fibers are then washed in distilled water for 24 hours to remove

any hydroxide residue. The annealing and hydrolysis processes are typically similar amongst the various researchers exploring PAN actuation unless otherwise noted.

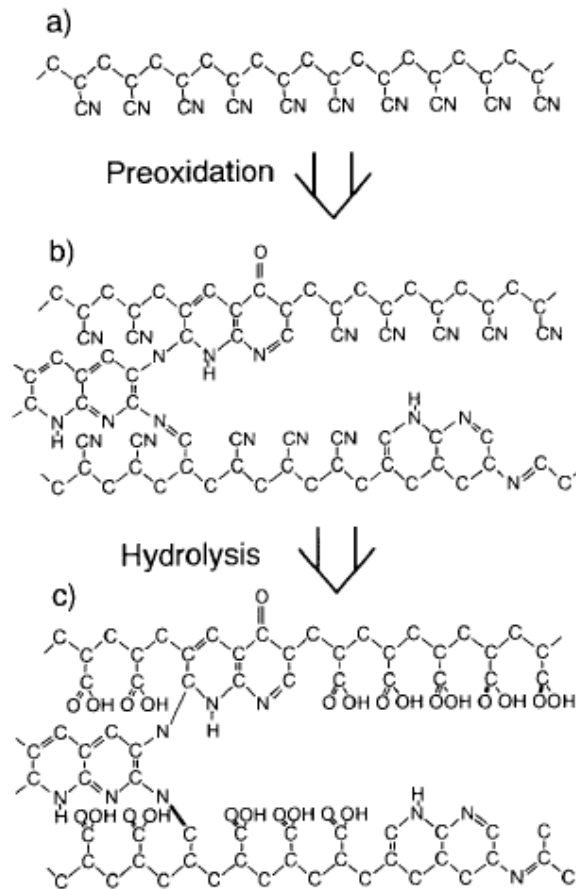


Figure 9: Schematic of the chemical structure of (a) PAN fibers; (b) pre-oxidized PAN fibers; (c) hydrolyzed PAN gel fibers [29]

2.3 Actuation Performance of PAN Fibers

Umemoto et. al observed activated PAN fibers to contract when exposed to acidic solutions and expand with exposure to alkaline solutions suggesting potential use as an artificial muscle actuator [29]. PAN fibers (22.5 μm diameter) were activated and performance characteristics under isotonic and isometric conditions were documented. The PAN fibers were stimulated using direct chemical exposure of various concentrations of NaOH and HCl solutions.

Correlation was found between the 'Aromatic Index' (AI) and peroxidation time as well as its effects on contract time and contract forces. AI represents the degree of ring structures present in the PAN fibers. As pre-oxidation times increased, an increase in pyridine ring structures are formed due to the evolution of hydrogen, cyclization of nitrile groups ($C\equiv N$), and crosslinking of chain molecules [25]. Activated PAN contracting from its expanded state shows a decrease in overall length change ($\frac{\Delta L}{L_0}$) and increase in contraction forces as the AI value increases. In other words, larger AI values are analogous to increasing stiffness of the material, showing smaller deflections yet supporting larger forces.

Unlike acidic and basic exposures, ion production due to electrolysis of water can stimulate the activated PAN. Shahinpoor suggested an electrochemical process to overcome the challenges posed by the use of high and low pH solutions [26]. pH is defined as the concentration of hydrogen ions present in a solvent or solution. As water is disassociated at the electrodes, hydrogen and hydroxide ions are formed, increasing and decreasing the pH, respectively. Since activated PAN is stimulated by pH, electrolysis provides a safer alternative for actuation as well as a means to control the degree of contraction and elongation using voltage.

Choe et. al fabricated an electrochemically driven PAN fiber bundle actuator to test actuation performance [30]. Thirty strands of pre-oxidized PAN fibers (220°C for 5 hours) were bound and saponified in LiOH. The activated fiber strands were then attached to a load cell to determine generated forces during contraction. Titanium mesh electrodes were used for the electrolysis process within 0.1 M NaCl solution. Isotonic testing was also conducted to determine the amount of work generated from the chemical and electrochemical actuation of the PAN fiber bundle.

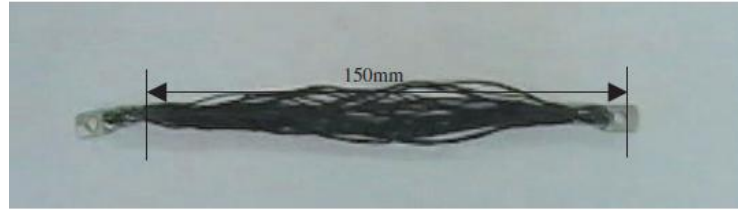


Figure 10: PAN sample [30]

The electro-chemically driven PAN bundle actuator managed to generate 80% of the maximum force produced by a similar chemically driven system within 30 minutes. The isotonic testing revealed chemical actuation generated work an order of magnitude higher than electrochemical work. Chemical actuation was completed within the first minute and electrochemical actuation was completed within 30 minutes (See Figure 11).

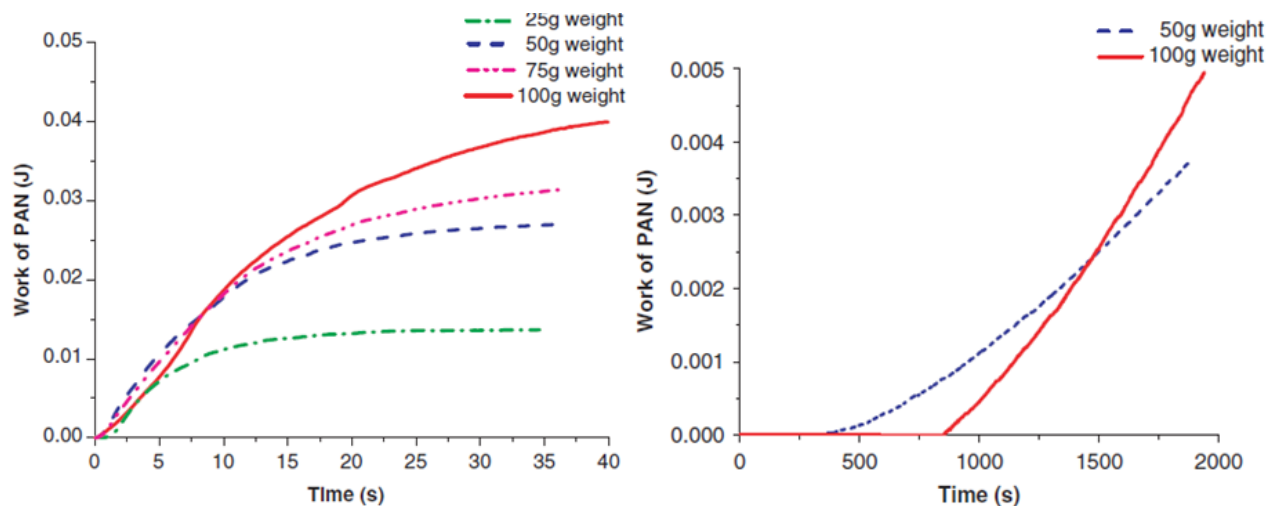


Figure 11: Work generated by chemical actuation (left) and Electrochemical Actuation (right) [30]

Shahinpoor addresses the long actuation times by comparing the PAN fibers to a diffusion controlled slab-type gel model provided below:

$$\frac{\Delta l}{\Delta l_0} = 1 - \sum_{n=0}^{\infty} \frac{8}{(2n+1)^2 \pi^2} e^{-\frac{(2n+1)^2 t}{\tau}} \quad (1)$$

$$\tau = \frac{4l_{ch}^2}{\pi^2 D} \quad (2)$$

Where $\frac{\Delta l}{\Delta l_0}$ is the normalized change in gel length, τ is the characteristic time of swelling, t is time, l_{ch} is characteristic length, and D is the overall diffusion coefficient of ions within PAN fibers [26]. If the characteristic length, instead of representing the thickness of a slab-like material, was associated with the radius of PAN fibers, the elongation rates would be dependent on fiber diameter. As a result, the elongation rates can be improved with smaller fiber diameters. Small diameter PAN fibers can be fabricated through an electrospinning process.

2.4: Electrospinning

Electrospinning is a high voltage process ranging from 5-50 kV that draws fibers from a polymer solution to be collected onto an electrically grounded collector plate. As the voltage applied to the syringe increases, the solution becomes charged and the electrostatic forces overcome the surface tension of the fluid, eventually forming a Taylor cone. From the Taylor cone, a jet of fluid is extruded once the threshold voltage is surpassed and the polymer solution begins to evaporate. The evaporation of the solution allows fibers to form as well as transfer the charge from the solution onto the surface of the polymer fibers. This charge transfer causes an abrupt change in the flow from the Taylor cone. A whipping effect occurs, forcing the fibers to elongate and stretch, progressively decreasing the fiber diameter. Typically, the fiber diameters can range from a few microns to a few nanometers.

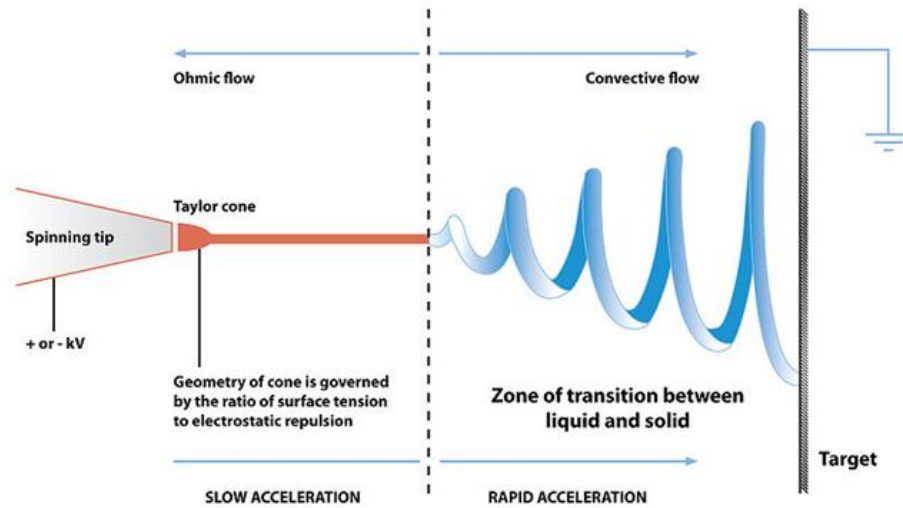


Figure 12: Behavior of Polymer solution during Electrospinning [31]

The use of nanofibers for actuation provides many benefits. Naraghi et. al examined the mechanical behavior of individual PAN nanofibers and found increasing elastic modulus with decreasing fiber diameters [32,33]. High molecular alignment found in nanofibers improved the fiber strength. Elastic moduli of 6 GPa were attained with fiber diameters of 200 nm (See Figure 13).

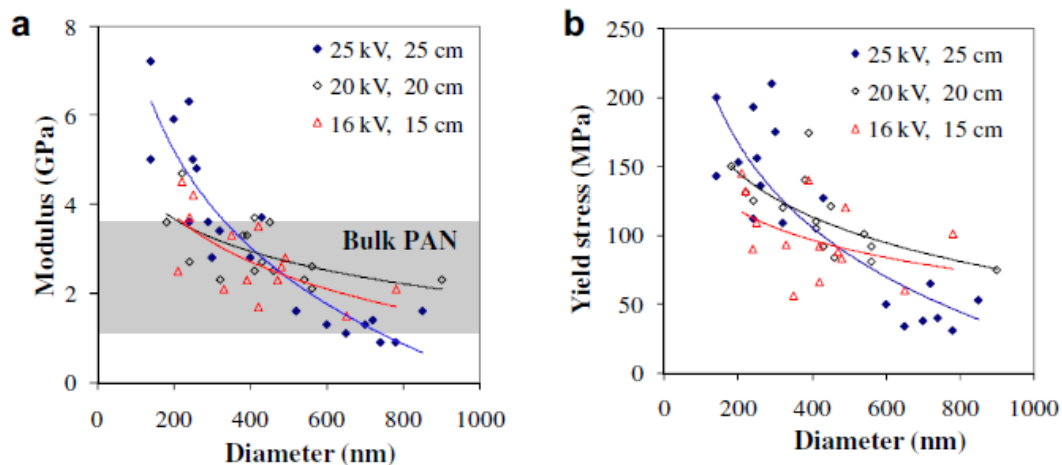


Figure 13: (a) Elastic modulus and (b) yield strength vs. nanofiber diameter for three electrospinning conditions. The range of modulus values for bulk PAN is shown in the shaded region in (a) [33]

Samatham recognizes fiber diameter plays a limiting role in solvent diffusion across the fiber. Thicker fibers require longer times to completely diffuse through the core, limiting the overall response time. Thus, reducing the fiber diameter will improve the response times, decreasing the duration needed to complete diffusion. Aside from fibril diffusion, nanofibrous structures are also preferred materials for improved permeability. [34].

The use of nanofiber mats also increases surface area [35-38]. Allowing chemical solvents or ions produced by electrolysis to be exposed to larger areas will improve response time necessary to saturate the fibers.

2.5: Parameter Effects on Electrospinning

The fiber diameter and fiber morphology are dependent on a large array of parameters. The electrospinning solution properties are one of the primary contributors affecting fiber diameter. Factors such as dielectric constant, conductivity, surface tension, viscosity, molecular weight, and solution temperature are taken into consideration when synthesizing the polymeric solution for desired fiber diameters. Understanding the roles each parameter plays toward fiber morphology will allow proper adjustments to the electrospinning apparatus to fabricate nanofibers with a desired range of diameters for the given application.

2.5.1: Concentration

Solution concentration is found to have a strong influence towards fiber diameter of electrospun nanofibers [39]. Various combinations of PAN concentrations (6-12 wt. %) and applied voltages (10-20 kV) were used for electrospinning and the resulting fibers were examined using a SEM. Fiber diameter decreased with lower concentrations and showed

consistent diameters, but beading along the fibers were present. Wang et. al mentions going below the minimum concentration that will form continuous fibers, the entanglement concentration, will produce nanoparticles instead. Higher concentrations yielded larger, non-uniform diameter fibers (See Figure 14). [35]

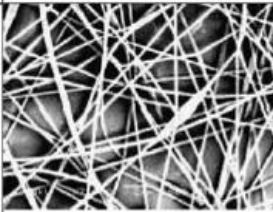
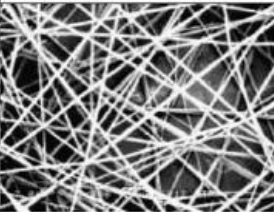
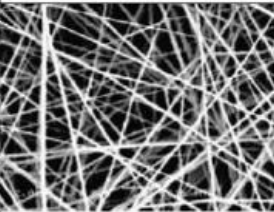
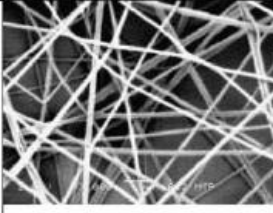
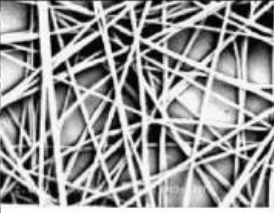
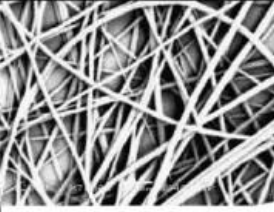
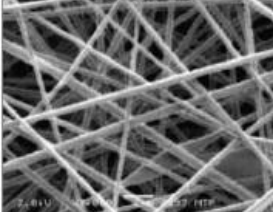
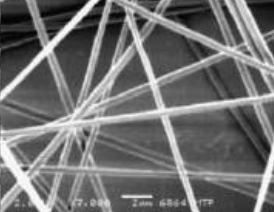
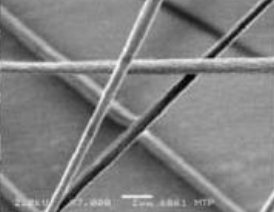
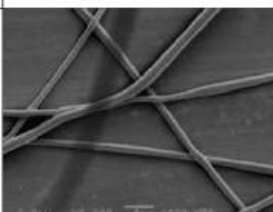
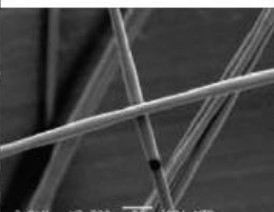
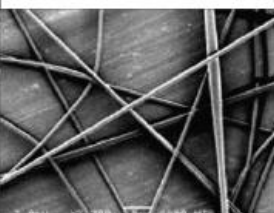
| Concentration (wt%) | Applied voltage (kV) | | |
|---------------------|--|--|--|
| | 10 | 15 | 20 |
| 6 |  214(44) |  213(46) |  208(39) |
| 8 |  290(66) |  290(53) |  291(63) |
| 10 |  394(69) |  436(176) |  472(70) |
| 12 |  1170(238) |  1160(267) |  1140(387) |

Figure 14: The morphology of fibers at applied voltage from 10 to 20kV at concentrations from 6% to 12% with a constant collector distance of 10 cm (The Values below the images and the brackets show the average fiber diameter (nm) and the standard deviation of fiber diameter. [39]

Between surface tension and viscoelastic forces, fiber morphology was found to be dependent on the most dominant force. At lower polymer concentrations, surface tension is the dominant force, minimizing surface area by forming beads along the fiber. Higher concentrations show viscoelastic force dominance, resisting bead formation and forming smooth fibers. Solution concentrations between 8-10 wt. % will provide relatively small, uniform PAN nanofibers.

2.5.2: Collection Distance

Naraghi et. al have found strong correlation between the fiber diameter and collection distance. As the collection distance is increased while maintaining the same electric field intensity, smaller diameter nanofibers develop [33]. As the polymer/solution jet requires longer time to reach the collector plate, an increased amount of solution is evaporating, increasing the viscosity. Increased viscosity induces larger shear stresses onto the polymer, improving molecular orientation and decreasing fiber diameter. Aside from the initial bending instabilities caused by the solution evaporation, additional instabilities may occur at long enough distances, further increasing solution evaporation, shear stresses, and molecular orientation.

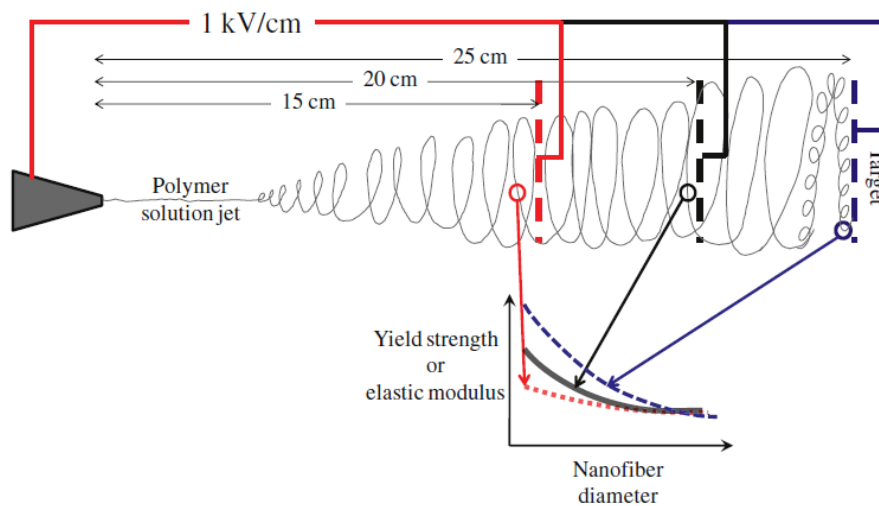


Figure 15: Schematic of the relationship between mechanical property size effects and electrospinning parameters. [33]

Aside from dependencies on fiber diameter and collection distance dictating mechanical strength, the concern of diffusion across PAN fibers is revisited. The preparation of the electrospinning solution requires dissolving PAN within a high dielectric solvent, saturating the PAN molecular chains. As PAN fibers are electrospun, residual solvent that does not evaporate remains trapped within the core of the collected fibers. The outer core of the PAN fibers condenses and solidifies whilst the inner core retains solvent molecules. [40]. Since the retained solvent was intentionally used as the polymer dispersant, it increases the plasticity of the material. Thicker fibers will retain more solvent and reduce the overall modulus of the fiber. Therefore, smaller diameter fibers will contain less solvent and provide better cross section uniformity, enhancing the modulus. [32]

2.5.3: Dielectric Solvent

Solution preparation requires a solvent with a high dielectric constant and conductivity. A high dielectric value intensifies the whipping effect as well as reducing the formation of beads, influencing nanofiber structure. In comparison to other dielectric solutions, Dimethylformamide (DMF) possesses a high dielectric constant (36.71) and highest conductivity (1.090 mS/m), eliminating the need to introduce salts to improve conductivity and create impurities into the nanofiber mats [41]. DMF also suspends carbon based particles very well, reducing agglomeration typically seen within water. This is preferred when incorporating conductive filler material to enhance strength and/or conductivity.

2.5.4: Humidity

The humidity of the local environment will influence the morphology of the collected fibers. The evaporation of the electrospinning solvent is necessary to extract the polymer fibers from the solution. High humidity will decrease the rate of evaporation and droplets may be collected onto the collector plate. Low humidity greatly affects high volatile solutions, rapidly evaporating the solvent and potentially causing clogging within the syringe needle [41].

2.6: Actuation Performance of PAN Nanofibers

Exploring the effect of fiber diameters on actuation rates, Gestos et. al actuated single hydrogel nanofibers by Atomic Force Microscopy (AFM) and reported significantly improved actuation rates. He suggests the slower actuation seen by Lee et. al [14] was due to the slow infusion of the solution into the bundled PAN fibers [42]. Samatham et. al electrospun nanofibers approximately 100 - 300 nm in diameter. Activated electrospun nanofibers were exposed to 1 M HCl to induce contraction. Instantaneous volume change was observed with over 100% change in length achieved [43].

Electrochemical actuation of PAN nanofibers hasn't been conducted or mentioned in the literature since Samatham in 2006 [44]. Exploring the design limitations and functions of PAN nanofibers may revive the pursuit of polymeric gel actuation for artificial muscle application. Addressing diffusion limitations, processing effects on mechanical properties and performance, and effects of electrochemical interactions will bring forth insight towards improving electrochemomechanical actuator systems.

Chapter 3: Chemical and Electro-Chemical Actuation Mechanism

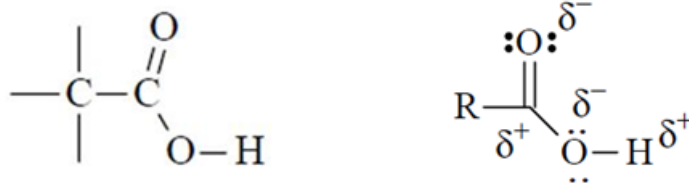


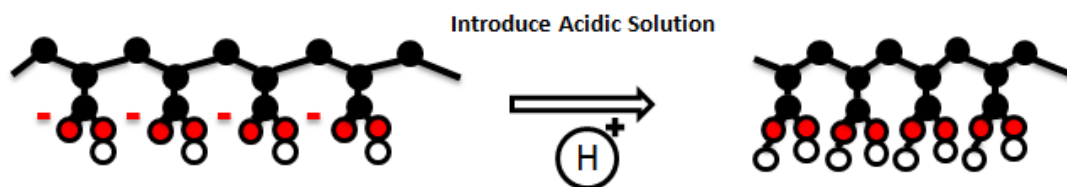
Figure 16: Carboxylic Acid and its dipole configuration (right) [45]

3.1: Activated PAN Fibers

Once PAN fibers have been activated, they become amphoteric and can accept and donate protons. This is due to the Carboxyl acid groups formed during hydrolysis. The acid group is comprised of a hydroxyl group (O-H) and a strongly polarized carbonyl group (C=O) (See Figure 16). Due to the strong polarization of the carbonyl group and oxygen's tendency to be electronegative, the negative charge typically resides with the oxygen atom. Thus, protons are attracted to the carbonyl group and protons can be donated from the hydroxyl group [45].

With many of the groups residing along the polymer chain in close proximity containing a dominant negative charge on the carbonyl group, electrostatic repulsive forces are present. The similar charges of the groups will repel from one another to restore equilibrium. The repulsive forces consequently force the polymer backbone chain to expand, expanding the whole polymer network. The electronegativity can be manipulated in order to expand and contract the polymer backbone (See Figure 17).

Contraction Phase



Expansion Phase

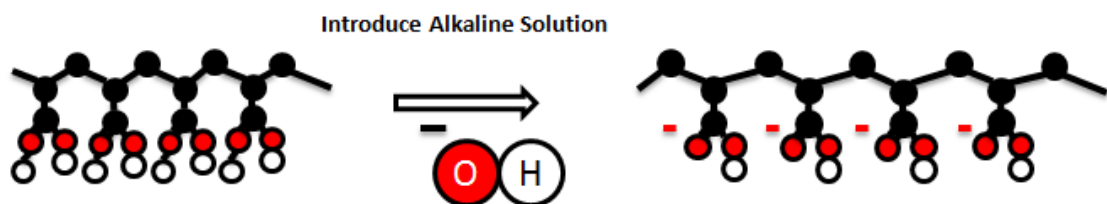


Figure 17: Simplified actuation mechanism of a single Activated PAN polymeric chain. The CPK coloring code is applied for Carbon (black), Oxygen (red), and Hydrogen (white)

3.2 Chemical Actuation

Introducing an acidic solution exposes the activated polymer chain to a high concentration of hydronium ions (H_3O^+). With the additional proton, hydronium ions are very reactive and can donate the excess proton to the Carbonyl moiety to stabilize into H_2O . This donation protonates the carboxyl acid group and redistributes the charge across the carboxyl group. With the carbonyl group no longer as strongly polarized, the overall charge of the carboxyl group is neutralized. This neutralization reduces the electrostatic repulsion forces, allowing the polymer chain to 'relax' and contract. Also, with the presence of additional hydrogen atoms, there may be subsequent hydrogen bonding between the carboxyl groups as well as bonding with nitrile groups found along the crosslinked polymer, enhancing the contraction effect.

This process can be reversed by exposing the activated polymer to a basic solution. Having a basic solution which has a dominant concentration of hydroxide (OH^-) ions present will

actively accept available protons. Since the carboxyl groups were introduced to additional hydrogen ions, they will relinquish the hydrogen ion, deprotonating the acid group. With the removal of the hydrogen, the distribution of charge across the group is disrupted, restoring the strong polarization to the carbonyl moiety. This charge restoration also restores the electrostatic repulsion, again stretching the polymer backbone to obtain equilibrium. Both the protonation and deprotonation occurs when a significantly acidic or basic solution is present.

Umemoto et al. observed abrupt contraction and elongation at different ranges of pH values [29]. The pH of the solution was decreased and increased in a step wise manner from pH 14 to pH 0 and vice versa. Abrupt contraction was shown at pH 3.7 as the pH decreased. As the pH increased, abrupt elongation was observed at pH 10.3. Lee et. al. also observed drastic change in contraction and elongation between pH 1-3 and pH 10-12, respectively. [14] This contraction/expansion process is characterized by a hysteresis loop and shows little to no degradation in performance. These findings suggest a pH threshold that must be met in order to

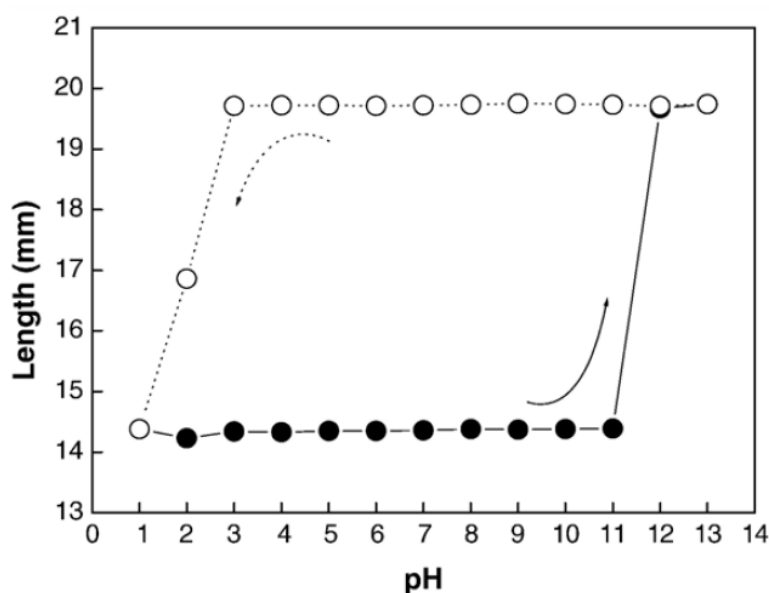


Figure 18: Hysteresis of Activated PAN fiber length vs. variation in pH [14]

begin the protonation and deprotonation process for actuation.

The contraction and expansion of the polymer network also causes changes in osmotic pressure within the system. Activated PAN fibers function like hydrogels, containing a significant amount of water or solution within its polymer network. When a low pH environment is present, the network will contract, resulting in the expulsion of solution from the network. When the contracted network is then exposed to a basic solution, the polymer network begins to expand. The expansion causes an inwards osmotic pressure, allowing solution to be re-absorbed into the network. It is believed this reabsorption assists in expanding the network.

Although acidic and basic solution actuation is shown to be effective, there are significant disadvantages for its use for fast actuation. Alternating acidic and basic solution exposure to the PAN fiber network can cause salt buildups, hindering the actuation capabilities. Many researchers have mitigated this issue by introducing an intermediary rinse cycle using water between chemical exposures. This process slows down the actuation process and would require a complex irrigation system to properly expose fibers and nanofibers to the appropriate solution. An alternative proposed by Shahinpoor et. al is to simulate the acidic and basic exposure using electrolysis. [26]

3.3 Electro-chemical Actuation: Electrolysis

Electrolysis can be utilized to create significant amounts of Hydrogen (H^+) and Hydroxide ions as the products of disassociating water or an electrolytic solution (See Figure 19). At the surface of each of electrode, the half reactions of water that occur are dependent on the direction of the applied voltage. At the anode, the positive end of the voltage supply is attached and draws electrons. Oxygen gas and hydrogen ions are evolved from the

decomposition of water at the anode. The hydrogen ions will react with water forming hydronium, resulting in an increased concentration of hydronium ions and increased solution acidity.

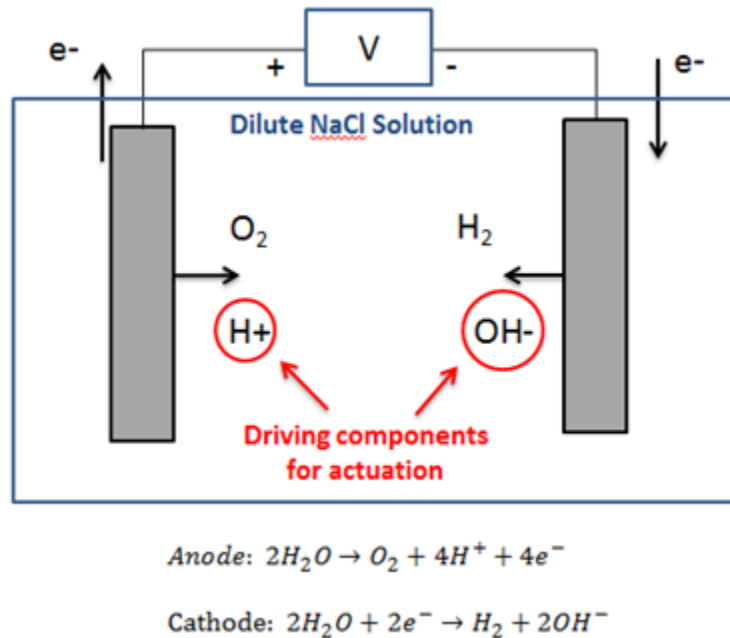


Figure 19: Electrolysis Half Reactions for water (Bottom) and Diagram with resulting Products (Top)

A similar process is seen at the cathode. The negative lead of the voltage supply is attached to the cathode, supplying electrons. Introducing electrons with water evolves Hydrogen gas and Hydroxide ions. An increased concentration of Hydroxide ions within solution increases the alkalinity of the solution. These changes in solution concentration change the pH value of the local solution, providing a means for actuation.

Even though the pH concentration changes are due to electrolysis, it is localized to the surface of the electrode. Due to the sudden change in pH, the concentration of ions will migrate from the electrode to stabilize. Flow effects caused by bubbling and pH of bulk solution contribute to forming a pH gradient dependent on the distance from the electrode surface. Bin et. al have examined this distribution of pH near the electrode surface using micro pH electrodes [46]. At 10 μm from the anodic surface within a solution of pH 6.42, the pH dropped

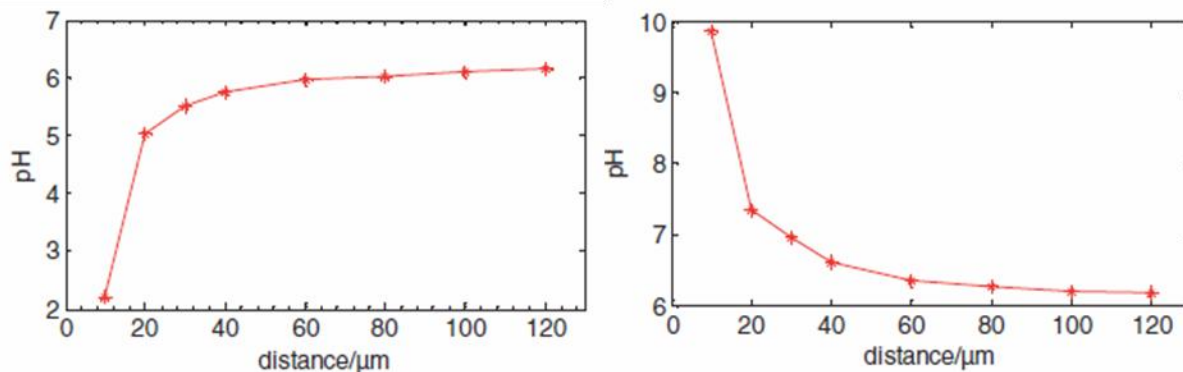


Figure 20: Distribution of pH near anodic surface (left) and cathodic surface (right) [46]

significantly to approximately 2 at +2.5V. At the same voltage and distance from the cathodic surface, the measured pH was approximately 10 (See Figure 20).

The significant change in pH value near the electrode surface (~10 μm) can be taken advantage of to actuate activated PAN nanofibers, addressing the potential pH threshold limitations shown in Figure 18. By maintaining close contact of the PAN nanofibers to the electrode, actuation can be triggered with an applied voltage. Metal deposition of Platinum onto the PAN fibers was suggested.

3.4: Improving PAN Fiber Conductivity

Shahinpoor et. al. introduced Platinum onto the fiber surface to increase the overall conductivity of the PAN nanofiber mat [26]. Due to the stiffness of platinum, the rate of

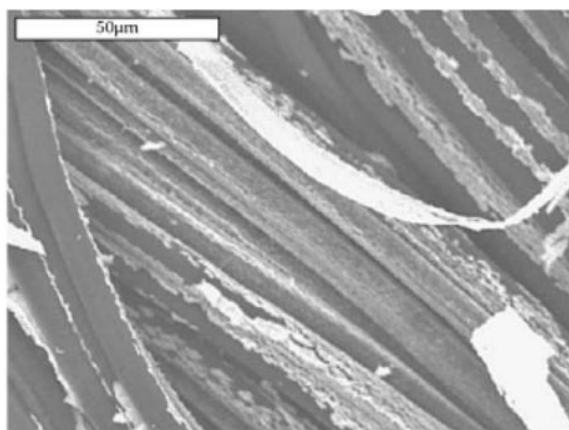


Figure 21: Delamination of Pt from PAN fibers [26]

elongation was significantly slower and deflection was reduced in comparison to the chemical reactions. Contraction and elongation rates were approximately 5%/min and 3%/min, respectively. Also, actuation cycling caused the deposited metal to delaminate from the fibers, requiring higher voltages to achieve the same strain percentage (See Figure 21). Graphite with gold counter electrodes was introduced to address the previous issues, significantly improving contraction rates by 100% and elongation rates by 67%.

An alternative to metal deposition and individually coiling graphite near PAN fibers is introducing conductive filler material to the nanofiber mats. Multi-walled Carbon Nanotubes, graphite, as well as conductive polymers have been explored as potential conductive filler material [47-49]. PAN is known to be an insulating material with conductivity ranging from 2 pS/m to 0.7 μ S/m [47]. By reducing the resistivity of the PAN nanofiber mat, it can be used as a conductive actuating hydrogel electrode [26]. The compliance of electrodes for this application is essential for minimizing the stiffness of the material as well as maintaining consistent electrical properties under high strain loading.

Common electrode materials such as platinum and silver have significantly higher conductivities of 9.43 and 63 MS/m, respectively [50]. This allows the material to transfer electrons through with minimal resistance. Since the electrolysis process requires the flow of electrons to operate, minimizing the resistance will increase the output of produced ions. Thus, it is critical to significantly improve the conductivity of the PAN nanofiber composite in order to maximize the ion production required to significantly change localized pH values.

Proper dispersion of conductive filler is essential to improve conductivity within PAN nanofiber mats. Carbon-based conductive filler requires proper dispersion techniques to prevent agglomeration. Van der Waal forces cause individual CNTs and graphite nanofibers to cluster

within solution. This clustering reduces the overall dispersion within the nanofiber mats and reduces the conductivity. Reducing the agglomeration will allow the conductive filler to be dispersed evenly, improving the likelihood of a continuous conductive network to exist within the nanofiber mat. Ultrasonication and high shear homogenization are typically implemented to mechanically disperse the conductive filler in solution. [47].

3.5: Activating Conductive PAN Nanofiber Composites for Actuation (Aims of Research)

Although the improved mechanical and electrical properties of PAN nanofibers embedded with CNTs are discussed here, no articles in the literature discussing the application of PAN nanofiber composites for actuation were found. The purpose of this research is to merge the efforts towards activated PAN nanofibers and the PAN/MWCNT composites and explore the co-electrospinning and activation of PAN with suitable conductive material to develop a composite actuator that contracts electrochemically (See Figure 22). The activated PAN composite will theoretically serve as an electrode, producing H^+ or OH^- ions within the nanofiber network, causing actuation.

The previous work done on electrospinning PAN nanofibers, activating the material, and chemically actuating the PAN nanofibers will be reproduced. The PAN nanofibers will then be electrochemically actuated using electrolysis. The electrospinning process will then be modified by introducing conductive material to the polymeric solution to prepare and activate nanofiber composite mats.

Electrical and mechanical testing will be conducted to characterize the composite material's performance. SEM imaging will be done to observe the nanofiber morphology, fiber diameter, and interaction with conductive materials. The conductivity of the material will be

examined to determine if the material would behave as an electrode and support electrolysis. Mechanical tensile testing of the contracted and expanded states of PAN will determine the relationship between the concentration of added conductive material and the resulting tensile properties of the composite. The parameters associated with the activation process are also examined for optimization purposes.

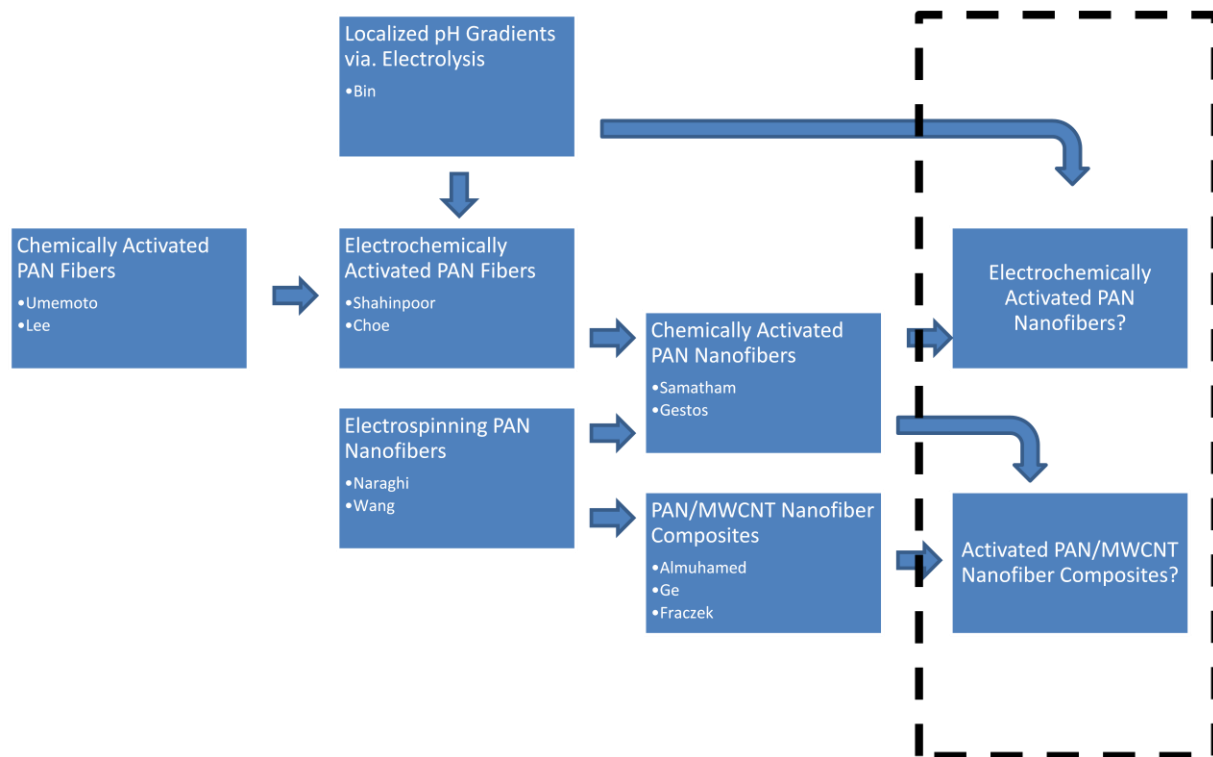


Figure 22: Flow chart of reliable research and associated authors on the methods of PAN actuation, the integration of the electrospinning process, and work done creating composite nanofiber mats with conductive material. The two highlighted topics represent the potential result of combining research efforts that have yet to be combined in available literature.

Chapter 4: Experimental Procedures and Results

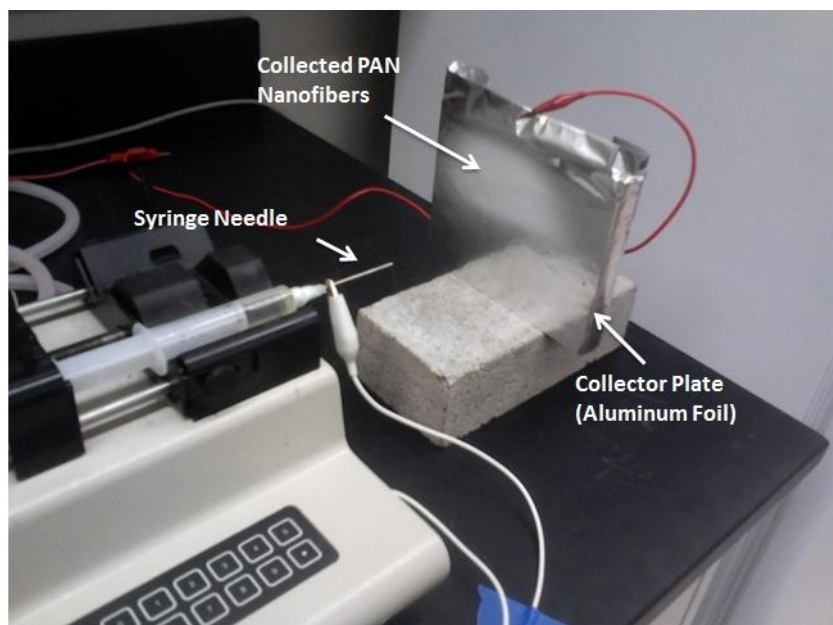


Figure 23: Horizontal Electrospinning Setup

4.1: PAN Nanofiber Fabrication

For all of the electrospinning experiments, both Polyacrylonitrile (PAN, $M_w = 150,000$) and Dimethylformamide (DMF) were purchased from Sigma Aldrich and used for all solution preparations. PAN was combined with DMF to create a 10% wt. solution and was mixed for 24 hours using a magnetic stir-bar. The solution changed from a clear solution with agglomerate PAN particles to a homogenized pale yellow solution with higher viscosity. Care was taken to minimize exposure to air to prevent the DMF from evaporating and increasing the %wt. of the solution.

A horizontal electrospinning setup was chosen to minimize the collection of excess solution droplets on the collector plate. As shown in figure 23, the setup consists of a high voltage power supply (10 kV), a syringe pump (KD scientific), a 2", 15 gauge stainless steel, flat tip needle, and a custom steel collector plate. The collector plate was covered with aluminum foil

for handling convenience. The positive lead from the power supply was attached directly to the base of the syringe needle and the ground was attached to the aluminum foil.



Figure 24: Close-up of Custom Collector Plate with Aluminum Foil

An electric field of 1 kV/cm was maintained with a collection distance of 10 cm. The flow rate was held at 0.763 ml/hr for 2 hours. Once the voltage was applied, a white circular film gradually appears on the center of the collector plate. PAN nanofibers were collected, eventually covering the entirety of the aluminum foil directly exposed to the electrospinning path. Small samples were extracted to examine the fiber diameter using a SEM (AMRAY 1830).

Following Schreyer's activation process, the electrospun PAN was annealed for 2 hours at 240°C [43]. To simplify the handling of the samples, the electrospun fibers remained on the aluminum foil and were removed after heat treatment. An ATS Series 3600 Oven was used for all annealing processing. Due to the oven's internal blower and the fragility of the PAN sample, the sample was placed on a baking sheet and covered with aluminum foil to prevent physical damage. Color change from white to dark brown was observed, indicating successful crosslinking [51]. The degree of crosslinking was observed using the SEM.

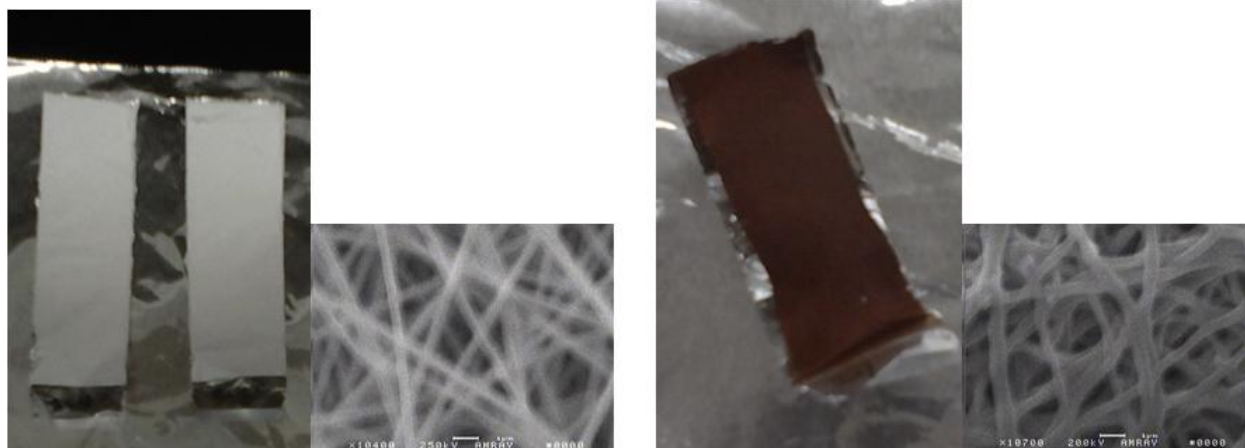


Figure 25: Pure PAN before (left) and after (right) heat treatment. SEM images show the effects of annealing on the crosslinking between PAN nanofibers.

Pre-oxidized PAN nanofibers were hydrolyzed within 1M Sodium Hydroxide (NaOH, Sigma Aldrich) at 95°C for 30 minutes. The temperature was reduced accordingly to minimize bubbling that may damage the samples. Activated samples were transferred to distilled water to remove excess NaOH solution over the course of 24 hours. Processed samples had a dark brown, near black appearance and had a texture consistent to wet seaweed.

4.2 Chemical Activation

To verify the activation process was successful, samples were exposed to 1N Citric Acid (HNO_3) to cause contraction and 1M NaOH to cause expansion. All measurements were made using a standard ruler. The initial length and width of the activated PAN sample was 4.5 cm and 1 cm, respectively. The contraction from exposure to HNO_3 from a NaOH solution showed an overall length of approx. 3 cm and width of 0.5 cm. Reversing the exposure expanded the sample to its initial length and width. A 33% decrease in length is achievable and by neglecting the change in thickness, a 67% decrease overall change in volume between NaOH and HNO_3 was achieved (See Figure 26).

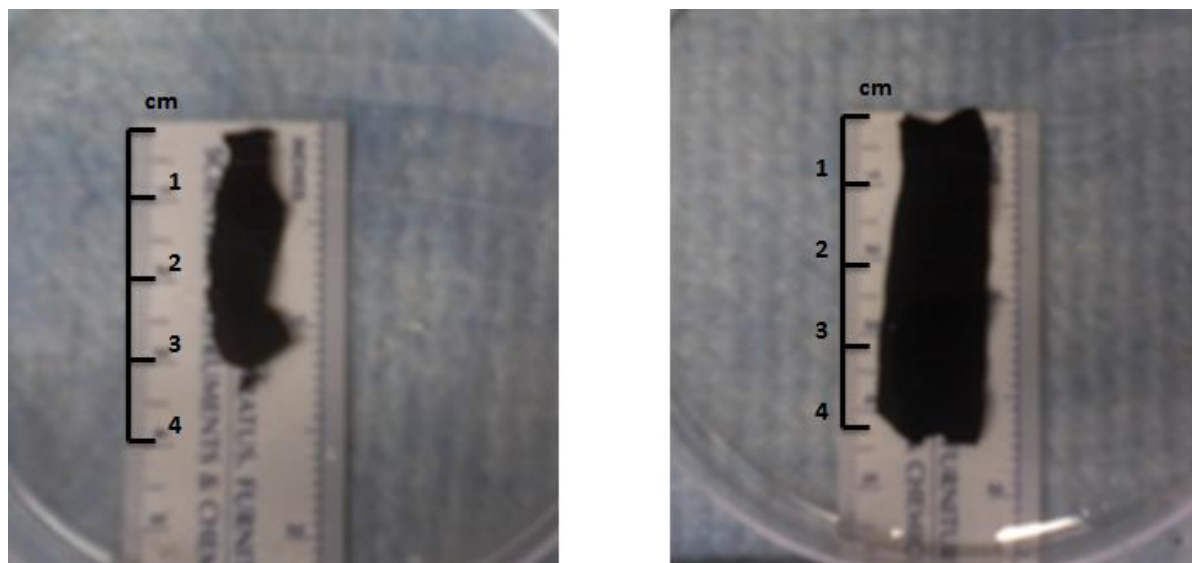


Figure 26: Chemical Activation using HNO_3 for contraction (Left) and NaOH for expansion (Right) Solutions. An enhanced scale has been added due to the image quality.

4.3 Electrochemical Activation

0.1 M NaCl solution was used as the electrolytic solution for the electrolysis process. A platinum wire and a platinum wire basket were the active electrodes in this setup. Due to the difficulty of handling the thin hydrogel samples, the platinum basket contained the sample to provide the necessary ions for actuation. A potential of +12.5 V was applied to the electrode basket for 5 minutes and the sample was promptly removed for examination. The sample was returned to the electrode basket and -12.5 V was applied.

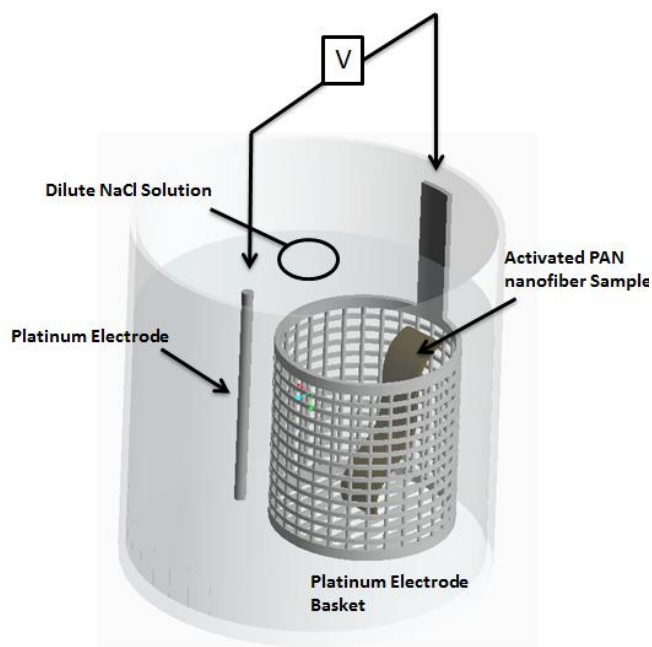


Figure 27: CAD model of the Electrochemical Actuation Setup

After the first 5 minutes of exposure to the anode, noticeable changes in shape were observed. Localized areas were contracted as well as discolored. The discoloration may be a result of hypochlorite formation due to the electrolysis of the NaCl solution. After the sample was returned and voltage switched, discoloration was reduced and the sample returned to its pre-contraction state.



Figure 28: Electrochemical contraction (Left) and Expansion (Right) of PAN Nanofibers.

The non-uniform contraction is the result of the amount of direct contact the sample made with the electrode. Since the significant changes in pH remain localized to the electrode, the areas of the sample that made direct contact with the electrode will be affected the greatest. The activated PAN sample tended to float within the basket and move due to the gas production of electrolysis. Measurements were not taken due to difficulty in confirming the average decrease in length and width. This observation emphasizes the necessity to maximize the amount of contact electrodes make with activated PAN nanofibers to significantly improve actuation capability.

4.4 Introduction of Conductive Additive to Electrospinning

To address the electrode contact issue, conductive additives were added to the electrospinning solution to improve the conductivity of the nanofiber mat and eliminate the need of stiff electrodes. Graphite nanofibers (200-500 nm dia.) and Multi-walled Carbon nanotubes (110-170 nm dia.) purchased from Sigma-Aldrich were used. Based on results published by Almuhammed to maximize volumetric electric conductivity, an electrospinning solution of 10% PAN and 1 % of MWCNT was used. [47]. Solutions of 10%PAN/5% Graphite and 10%PAN/5%MWCNT were also tested. PAN and the selected conductive additive were combined and DMF was added. The solution was mixed using a electromagnetic stir-bar for 24 hours and followed with sonication for 30 minutes. Due to the volatility of DMF, the solution was contained and held within an ice bath to prevent solution evaporation

The solutions were electrospun for 2 hours at 0.768 ml/hr, using a 10 cm collection distance, and with a 1 kV/cm electric field. Electrospun samples were activated using the same

process described in section 4.1. Samples were extracted before and after annealing for SEM analysis.



Figure 29: Top view of 90% PAN/10% MWCNT (left) and 66% PAN/33% Graphite (right) collected onto aluminum foil

During the electrospinning process, a 3D nanofiber mound of PAN nanofibers and MWCNTs began forming on the collector plate. Reducing the flow rate prevented 3D formations and provided a flat, uniform collection of fibers similar to previous electrospinning samples. The 1% MWCNT sample had a gray color with a white outline. The separation of the polymer from the conductive additive may be due to the influence of electrostatic forces on the MWCNTs. 5% MWCNT and 5% graphite samples were black due to dominating carbon content. Little color change was observed after annealing.

Following hydrolysis, the samples became very amorphous and difficult to handle. Due to the conductive additives, the PAN nanofibers had a less dense network for crosslinking. The integrity of the nanofiber mat was reduced, weakening the structure.

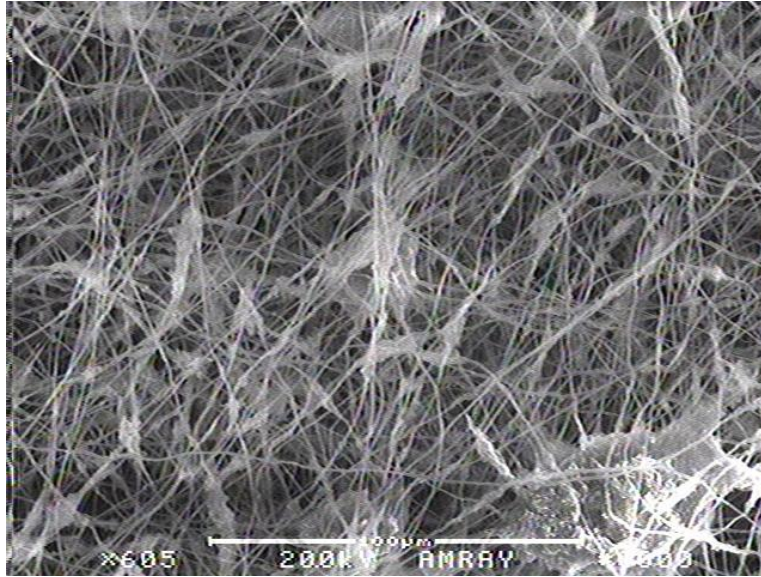


Figure 30: Significant Agglomeration of 10% PAN/ 5% MWCNT SEM sample (Scale 100 μ m)

SEM analysis shows significant agglomeration of conductive additive material (Figure 30). This agglomeration is known to increase the percolation threshold, decreasing the overall conductivity of the material [47]. Figure 31 depicts interwoven conductive nanofibers, signifying potential of individual nano-electrodes generating ion locally to each PAN nanofiber. Until further studies are done on the integration of conductive filler material, alternative means of conduction were investigated.

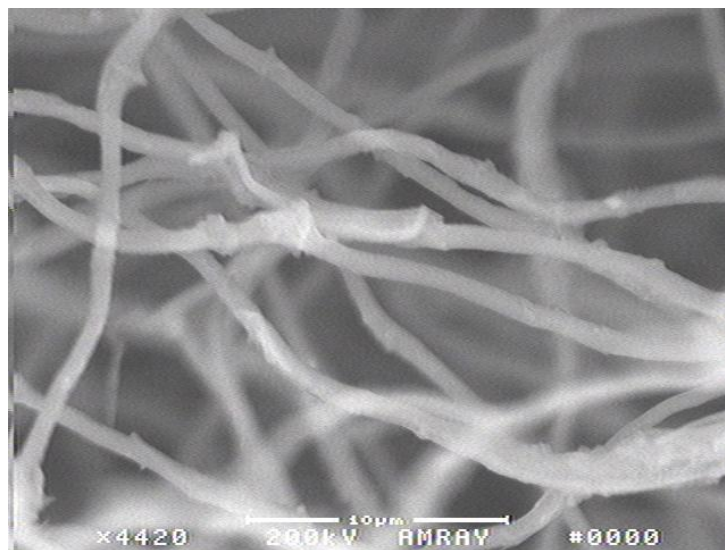


Figure 31: PAN and Graphite Intertwined Nanofibers (Scale 10 μ m)

4.5 Alternative Conductive Electrode Materials

Two considerations for alternative conductive material are conductive graphite sheets and graphite aerosol. PGS Graphite sheets (Panasonic) with a thickness of 25 μm were purchased and used as is for all testing. Dry Graphite Aerosol Spray Lubricant (Asbury Carbons) advertised to improve conductivity was tested on un-treated silicon wafers. Various spray times were implemented to determine the effect of graphite thickness on conductivity (See Table 4). Silicon wafers were held approximately 12" from the spray nozzle and were allowed to completely dry prior to conductivity testing. Thickness was determined through SEM analysis (See Figure 32).

Conductivity of both materials was measured using the four point probe method. Since the thickness of the sample layer was much less than the spacing between each probe, the following equation is applied to calculate the sheet conductivity σ measured in Siemens per meter:

$$\sigma = \frac{\ln 2}{\pi t} \left(\frac{1}{R} \right) \quad (3)$$

Where t is sheet thickness and R is measured resistance. Thickness was determined from SEM images of each sample.

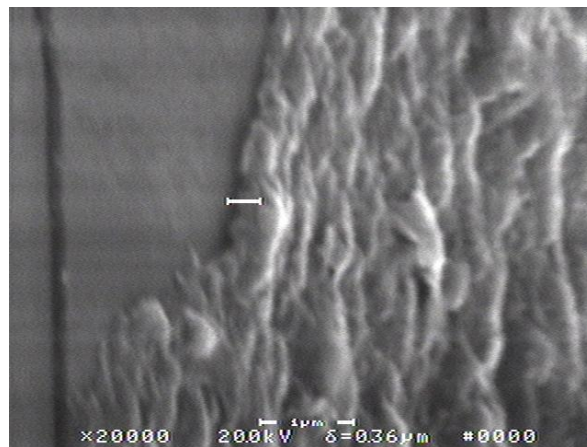


Figure 32: SEM Image of Graphite deposited onto Silicon Wafer. Spray time = 1.0 sec

Both materials were also subject to electrolysis testing to determine its ability to disassociate water. 0.1 M NaCl solution and a graphite electrode were used for all tested electrode samples.

Table 4: Conductivity vs. Spray Time

| Spray Time (sec) | Avg. Thickness (μm) | Conductivity (S/m) |
|------------------|----------------------------------|--------------------|
| 0 | 0 | 0 |
| 0.5 | 0.3 | 2.9 |
| 1.0 | 0.4 | 0.9 |
| 1.5 | 0.8 | 16.0 |
| 2.0 | 4.2 | 1.6 |
| 2.5 | 12.2 | 0.4 |
| 3.0 | 17.4 | 0.1 |

Of the tested samples, a 1.5 second spray time yielded the largest sheet conductivity of 15.95 S/m. A noticeable characteristic amongst all samples was uneven graphite layering. The solvent suspending the graphite evaporated off of the wafers unevenly, resulting in varying thicknesses across the substrate. Multiple measurements were taken across a sample to create an average conductivity.

Between the two media, the graphite sheet had the best conductivity of 7.8 kS/m. During electrolysis testing, the graphite sheet electrode successfully disassociated water. However, all of the graphite aerosol samples could not conduct within solution. Further investigation into aerosols containing conductive material may be warranted as an alternative method of improving conductivity of PAN composites.

4.6 Transient variation of Localized pH

Bin emphasized the effects of distance on changes in localized electrode pH [46]. Improving actuation rates requires the examination of time dependencies on pH variation. The intended design for PAN actuators is to have active electrodes in direct contact with activated PAN nanofibers. Minimizing the limiting effect of distance promotes greater dependency on time and voltage for electrolytic ion production.

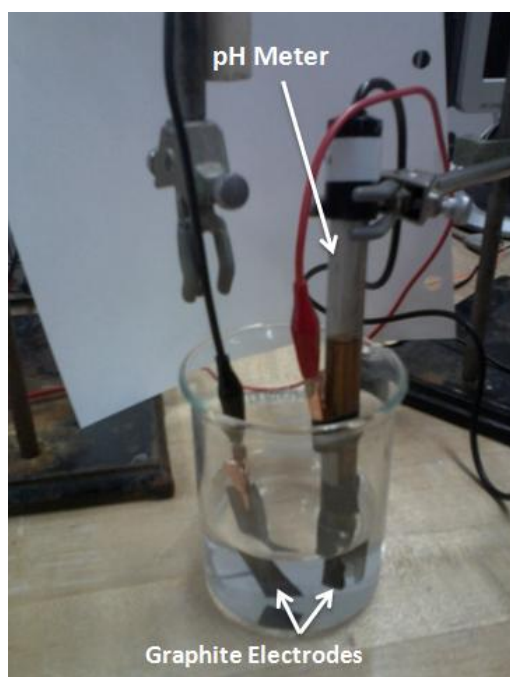


Figure 33: Electrolysis Setup for localized pH measurements over time

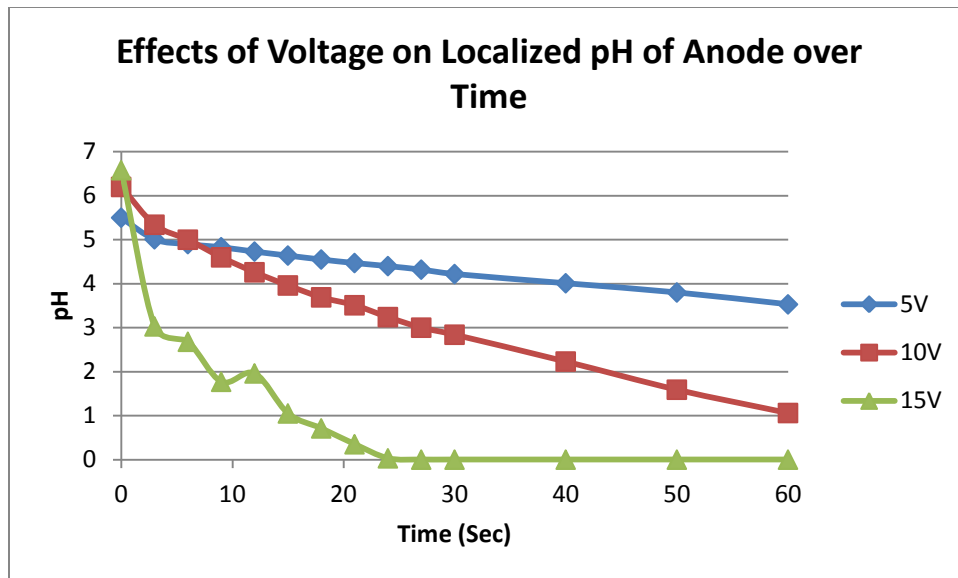
Two graphite sheet electrodes were placed within a 0.1M NaCl solution for the electrolysis process. One electrode was attached to a pH meter (See Figure 34) in such a way as to make direct contact with the glass probe. The pH meter was calibrated using pH 7 and pH 4 buffer solutions as the attached electrode would be the active anode producing H^+ , decreasing pH levels. For cathode operation, the pH meter was recalibrated using pH 7 and pH 10 buffer solution for increasing pH levels. Applied voltage was held constant for 1 minute durations and

pH values collected throughout each duration (See Figure 35a & 35b). The testing solution was stirred to restore the initial pH equilibrium prior to retesting at new voltages.

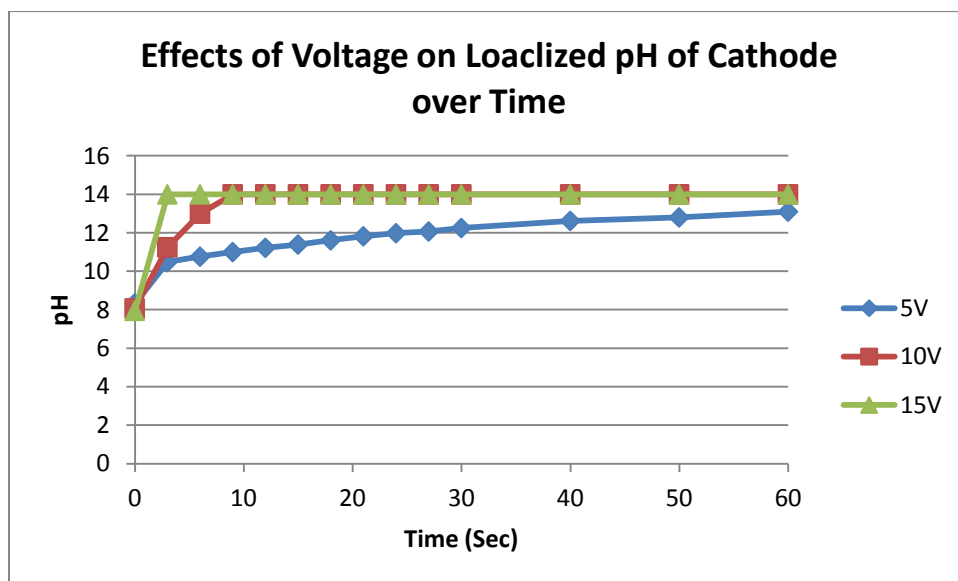


Figure 34: pH Meter with attached Graphite Sheet Electrode

As the voltage increased, the pH decreased at faster rates. At 15V, 3 pH was achieved within the first 3 seconds and 0 pH was reached by 27 seconds. The pH change was more dramatic for the active cathode. An applied voltage of 10V produced 11.25 pH within 3 seconds, surpassing 14 pH within 9 seconds. 15V yields a pH of 14 within the first second of operation. Increasing voltage would drive H^+ production up, further reducing the pH drop at the anode.



a)



b)

Figure 35: pH vs. Time

4.7 Processed PAN Nanofiber Tensile Testing

Tensile testing was administered to PAN nanofibers before and after the hydrolysis process. Variation in annealing time was applied to observe effects crosslinking has on the

mechanical strength and strain capabilities throughout activation processing. To improve handling, samples were electrospun for 6 hours with the same parameters mentioned in Section 4.1. The thickness of the samples ranged between 0.007" and 0.015". Testing was done on samples with annealing times of 1.5, 2.0, 2.5, and 3.0 hours. The average mass of the tensile samples was 35.6 ± 1.7 mg. From SEM analysis, the average fiber diameter was 490 ± 40 nm. Testing was conducted on the MTS Sintech Model 1125 Tensile Tester using a 50 kg load cell.

Each test sample's gage area measured 2" x 0.75" prior to hydrolysis. The samples not hydrolyzed had electrical tape applied to the grip sections to improve gripping within the tensile tester. For samples to be hydrolyzed, the grip sections were bound with Polydimethylsiloxane (PDMS) to improve grip traction and handling whilst withstanding high alkalinity treatment (See Figure 37).



Figure 36: Annealed PAN nanofibers with increasing duration from left to right prepared for tensile testing



Figure 37: Hydrolyzed PAN samples with PDMS Grip Sections

Sylgard[®] 184 Silicone Elastomer was applied to the PAN samples within a custom mold. The samples were cured at 130°C for 40 minutes and then hydrolyzed for 30 minutes. Since there is no standardized testing method available for hydrogel nanofibers, a custom procedure is used to test the contracted state of the material. Hydrolyzed samples tested under contraction were prepared by exposure to HCl, followed by a rinsing phase in distilled water to remove excess acid. Measurements before and after acid exposure were made. The length and width of hydrolyzed sample varied due to the uptake of water during the rinsing process. Prior to each tensile test, excess water was removed from all wet samples.

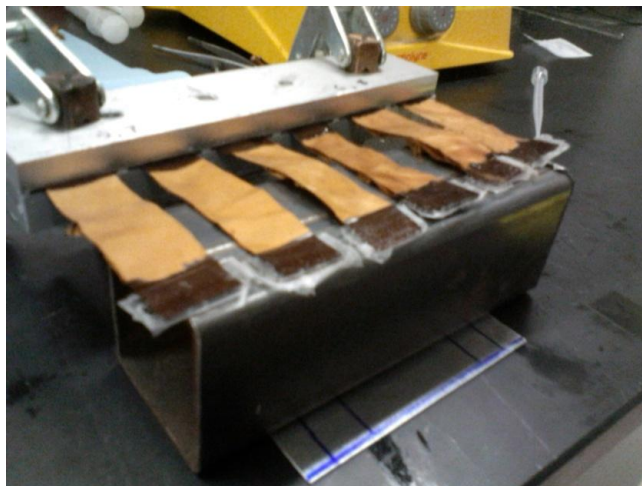


Figure 38: PDMS Grip Section Casting of Pre-oxidized PAN Samples in Custom Mold

A 0.05 in/min strain rate was applied to the dry samples and 0.2 in/min applied to the wet samples. Higher strain rates for the wet samples were used to prevent stress relaxation as well as excessively long testing that may dry out the samples.

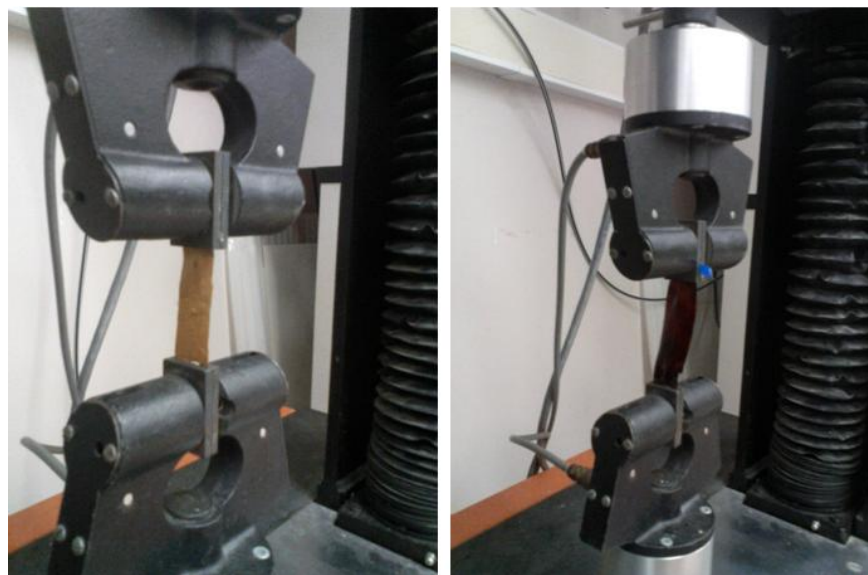


Figure 39: Tensile Testing of Dry Samples (Left) and Wet Expanded Samples (Right)

The variation of color amongst the samples progressed from a light tan for shortest annealing times to a dark brown for the longest annealing times (See Figure 36). The dry samples showed no necking upon failure. The samples showed low ductility as well as near clean breaks perpendicular to the applied load. A few samples showed shearing between layers,

indicating layer delamination due to poor layer crosslinking. The impact of annealing times on ultimate stress and maximum strain is summarized in Tables 5-7. Of the dry samples, the 2.5 hour heat treatment provided the greatest average ultimate stress and maximum strain at 3.6 MPa and 7.3%, respectively.

Table 5: Pre-oxidized Sample Tensile Data

| Pre-Oxidized Samples | | | | | | | | | | | | |
|-----------------------|--|--------|-----|--------|-----|--------|------|--------|--------------------|-----|-----|------|
| Annealing Time (hour) | Ultimate Stress (MPa) (<i>Young's Modulus {kPa}</i>) | | | | | | | | Maximum Strain (%) | | | |
| | 1 | | 2 | | 3 | | Avg. | | 1 | 2 | 3 | Avg. |
| 1.5 | 3.4 | (53.4) | 4.1 | (102) | 2.9 | (130) | 3.5 | (95.2) | 4.9 | 5.7 | 5.9 | 5.5 |
| 2.0 | 1.4 | (123) | 2.3 | (139) | 1.5 | (149) | 1.8 | (137) | 4.0 | 5.5 | 4.8 | 4.8 |
| 2.5 | 3.8 | (63.4) | 3.1 | (22.7) | 3.8 | (107) | 3.6 | (64.3) | 6.1 | 8.8 | 6.8 | 7.3 |
| 3.0 | 4.7 | (140) | 3.4 | (41.7) | 2.2 | (53.5) | 3.4 | (78.4) | 5.3 | 7.0 | 5.3 | 5.9 |

Table 6: Expanded Hydrolyzed Sample Tensile Data

| Hydrolyzed (Expanded) Samples | | | | | | | | | | | | |
|-------------------------------|--|--------|------|--------|------|--------|------|--------|--------------------|------|------|------|
| Annealing Time (hour) | Ultimate Stress (MPa) (<i>Young's Modulus {kPa}</i>) | | | | | | | | Maximum Strain (%) | | | |
| | 1 | | 2 | | 3 | | Avg. | | 1 | 2 | 3 | Avg. |
| 1.5 | 0.04 | (0.69) | 0.04 | (0.91) | 0.02 | (0.82) | 0.03 | (0.80) | 48.5 | 37.7 | 26.6 | 37.6 |
| 2.0 | 0.04 | (0.55) | 0.01 | (0.45) | 0.04 | (0.84) | 0.03 | (0.61) | 35.3 | 29.3 | 32.7 | 32.4 |
| 2.5 | 0.11 | (1.60) | 0.05 | (1.11) | 0.09 | (1.83) | 0.08 | (1.51) | 38.6 | 32.0 | 35.2 | 35.3 |
| 3.0 | 0.05 | (0.94) | 0.04 | (0.70) | 0.03 | (0.75) | 0.04 | (0.80) | 40.1 | 45.8 | 42.3 | 42.7 |

Table 7: Contracted Hydrolyzed Sample Tensile Data

| Hydrolyzed (Contracted) Samples | | | | | | | | | | | | |
|---------------------------------|-------------------------------------|--|--------|------|--------|------|--------|--------------------|------|---|-------|--|
| Annealing Time (hour) | Avg. Initial Length Contraction (%) | Ultimate Stress (MPa) (<i>Young's Modulus {kPa}</i>) | | | | | | Maximum Strain (%) | | | | |
| | | 1 | | 2 | | Avg. | | 1 | 2 | - | Avg. | |
| 1.5 | 58.8 | 19.8 | (23.4) | 18.9 | (32.7) | 19.4 | (28.0) | 131 | 118 | - | 124.5 | |
| 2 | 55.5 | 121 | (68.9) | 33.3 | (103) | 77.1 | (86.0) | 128 | 95.8 | - | 111.9 | |
| 2.5 | 47.5 | 39.6 | (248) | 26.4 | (166) | 33.0 | (207) | 84.5 | 74.4 | - | 79.5 | |
| 3 | 45.5 | 11.5 | (225) | 11.7 | (168) | 11.6 | (197) | 53.6 | 68.0 | - | 60.8 | |

Tensile testing of the expanded hydrolyzed samples displayed elastomeric stress-strain behavior. High deflection under low loads was observed with no necking or dramatic volume change. Failures occurred in the same lateral manner as the dry samples. Three hour annealing times showed abrupt changes in stress during testing. Progressive failure of the sample's layers resulted in transferring the load onto the remaining intact layers until complete failure. Upon inspection, no permanent deformation was found amongst the expanded samples. The greatest average stress was produced by 2.5 hour heat treatment, but the greatest strain was produced by the 3.0 hour sample.

Contacted hydrolyzed samples showed significant degrees of initial contraction due to the acid exposure. The contraction strengthened the fiber layers, allowing a dramatic increase in load capacity. Strain capabilities were also improved, reaching upwards of 131%. Plastic deformation was evident upon examining the samples after testing. As the samples began plastically deforming, striations formed due to fiber realignment with the direction of load. A majority of the samples showed very linear stress – strain plots. As annealing time increased, the linearity of the stress-strain plots decreases and the material behaves less like an elastomer.

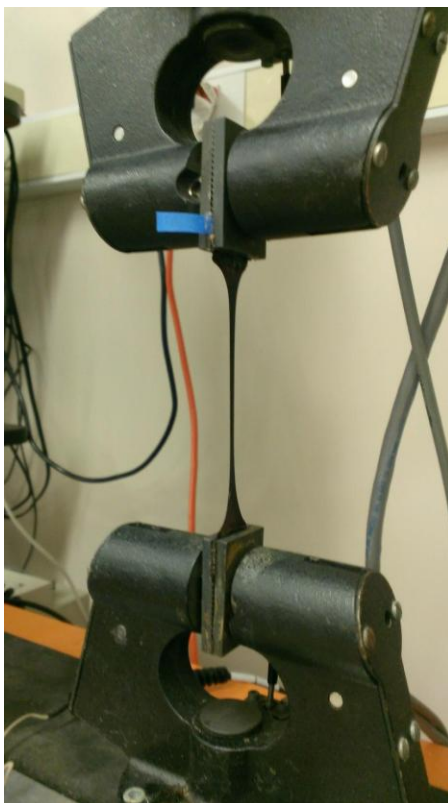


Figure 40: Tensile Testing of Wet Contracted PAN Nanofiber Mat

As shown in figure 42, as annealing time increases, the amount of contractile displacement decreases. Due to the increasing pyridine groups formed from pre-oxidation, the contraction potential diminishes with the decrease in available carboxylic acid groups. Annealing times beyond 3 hours at 240°C will remove most nitrile groups, forming cross-linked PAN that would be unresponsive to acidic or basic stimuli after hydrolysis.

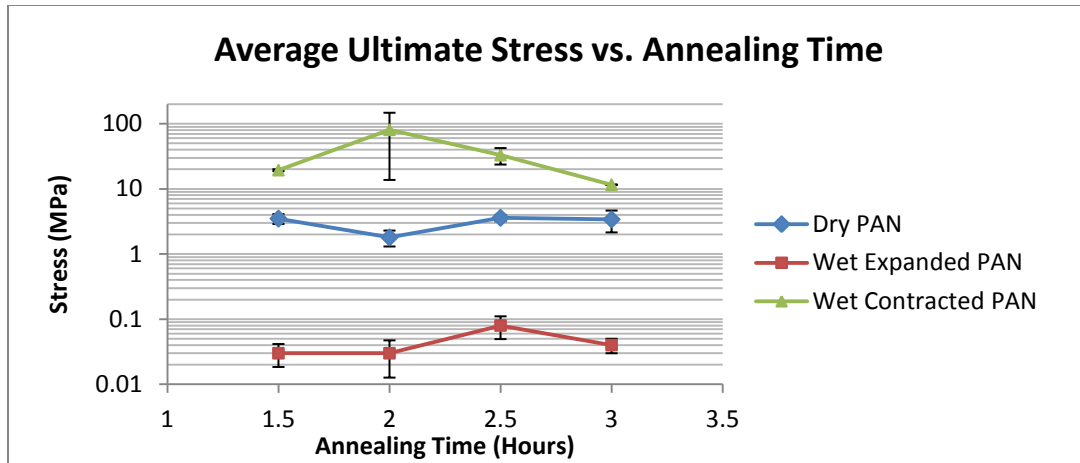


Figure 41: Effects of Annealing Time on Ultimate Stress

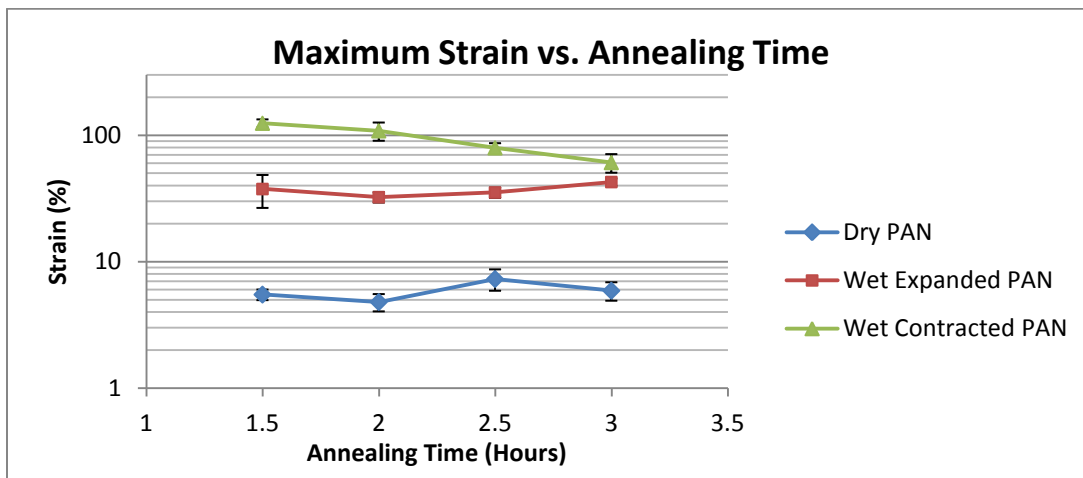


Figure 42: Effects of Annealing time on Maximum Strain

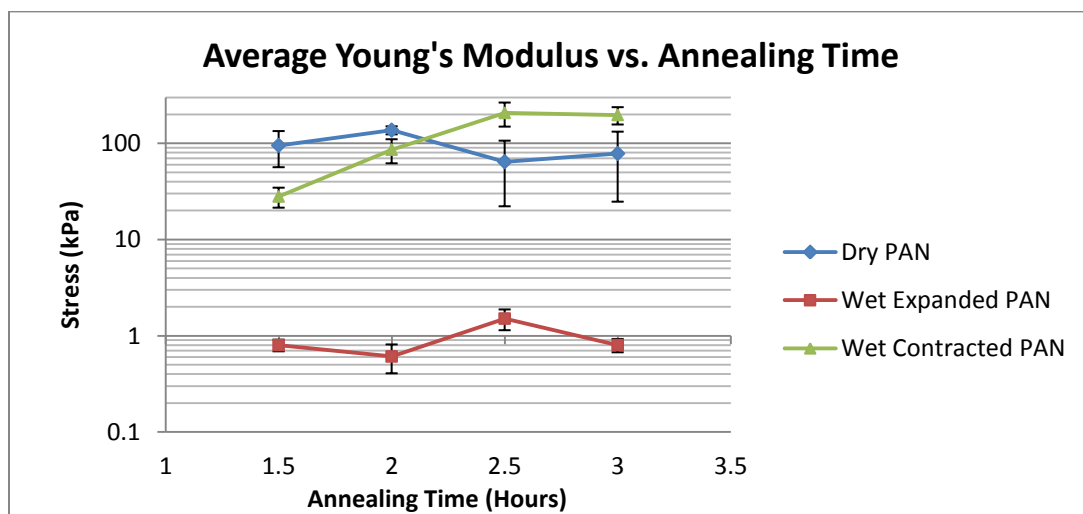


Figure 43: Effects of Annealing Time on Young's Modulus

The hydrolysis process significantly reduces the elastic modulus of the PAN nanofiber mats. Nearly two orders of magnitude difference is shown in Figure 43. As annealing times increase, the resulting stiffness for contracted PAN nanofibers increases, peaking at 207 kPa.

Variations in tensile testing could be attributed to a few factors. Due to the electrospinning process, the fibers are collected onto a fixed plate. This configuration will cause a greater density of collected fibers at the center of the collector plate, varying the thickness. Stress vs. Strain plots are provided in Appendix C.

4.8 PAN/Graphite Composite Actuator (Prototype I)

The results from the alternative electrode testing (See Section 4.5) and the PAN nanofiber tensile testing (See Section 4.7) have influenced the design of the PAN/Graphite composite actuator to maximize actuation performance. 10% wt. PAN/DMF was electrospun for 2 hours and annealed for 2.5 hours. Two PAN nanofiber samples 3" x 0.75" were prepared and enclosed a PGS graphite sheet electrode of the same dimensions. The composite layers were held together with PDMS in the same manner used to prepare the gripper sections for the hydrolyzed tensile samples. Upon activation, a copper lead was attached to the inner graphite electrode. The PAN composite was fully immersed within 0.1 M NaCl solution alongside a graphite electrode. +10V were applied for 5 minutes to the PAN composite. The voltage was reversed after an intermediate examination.

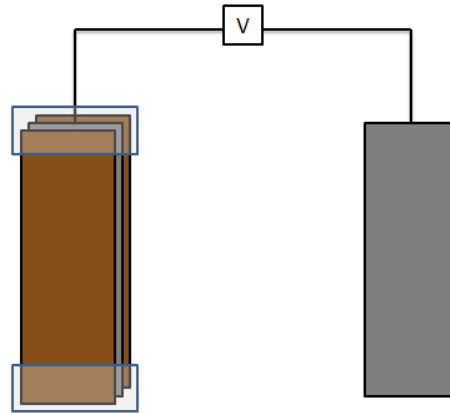


Figure 44: PAN/Graphite/PAN configuration for electrolysis

The PAN/Graphite/PAN composite showed significant contraction and curling. The composite linearly contracted 10% and sustained a width reduction of 40%. Localized areas showed discoloration and contraction. Due to the lack of adhesion between the layers, the PAN layers had maximal contact near the grip sections and almost no contact near the center, slowing the actuation process. As the PAN layers contracted, buckling was observed from the electrode. The buckling created higher surface contact with the unaffected sections of PAN and induced contraction. Once the voltage was reversed, the sample returned to its initial state.



Figure 45: Graphite electrode buckling within PAN/Graphite/PAN composite

4.9 Modifications to PAN/Graphite Composite Design (Prototype II)

To reduce the layer separation during electrolysis, sample preparation was modified. PAN was electrospun for 2 hours and the process was paused. A graphite sheet electrode with spring-like geometry was placed over the electrospun nanofibers (See Figure 46 & Appendix F). The spring geometry would allow for greater deflection and minimize buckling. The electrospinning was continued for another 2 hours, allowing the PAN nanofibers to completely envelope the graphite electrode. The sample followed the same activation procedures as the first composite design and tested within the same conditions.



Figure 46: Modified Electrode Design applied to Electrospun Sample

Significant improvements in contraction were observed within the first minute of electrolysis at +15V. A 25% length decrease and 37% width decrease was observed. Reversing the voltage resulted in a delamination of the PAN layers. Excessive bubbling caused the thin nanofiber film to fail and decreased electrode contact. The graphite electrode showed signs of swelling and degradation, resulting in electrode failure. Bubbling may have caused diffusion across the electrode as well as pressure buildup within the PAN composite.



Figure 47: Modified PAN/Graphite/PAN in contracted state

Chapter 5: Discussion of Results

5.1: Conductive Additives

Handling difficulties of PAN/MWCNT and PAN/Graphite samples potentially resulted from incomplete crosslinking of the PAN fiber layers. As the electrospun fibers are collected, the nanofibers rest on top of one another. Similar to the "fluffy" 3D structures formed on the collector plate, the density of the conductive PAN mat would be less than the pure PAN mat. Low density nanofiber mats would produce weak crosslinking between the layered fibers during annealing. Longer heat treatments may improve crosslinking, but the strain capabilities diminish for long annealing times.

SEM analysis has shown persistent agglomeration of conductive material within the PAN nanofiber mats. Consequently, the conduction of the samples was unobtainable due to the high resistance. Although the sonication process was included in the preparation of the solution, additional processing may be necessary to minimize agglomerates from forming. PAN is naturally insulating with an electrical resistance of approximately 1.5×10^{-12} S/m, requiring at least twenty orders of magnitude improvement to have conductivities comparable to various metals [47]. Surfactants and surface functionalization of Carbon nanotubes may enhance the MWCNT and graphite dispersion. The difficulty of introducing additional constituents to the electrospinning is changes to the solution properties, requiring adjustments to the electrospinning setup parameters.

CNTs are classified as 1D-conductors in the axial direction. To enhance the conductivity of a material, unidirectional alignment of CNTs will greatly improve performance. From the

observation of MWCNTs intertwining with PAN nanofibers, orienting the PAN nanofibers will align the MWCNTs, potentially improving conductivity.

5.2: Alternative Electrode Materials

Oxygen production during electrolysis at the graphite electrode causes erosion, forming a carbon dioxide byproduct. As a result, the life of a graphite electrode is determined by the applied voltage and amount of O₂ produced. Inert materials would be preferred for electrolysis applications. Due to high fluctuations in pH, high corrosive resistance is desired to prevent premature failure as well as production of by-products.

The electrochemical actuation of Prototype I resulted in a significant amount of electrode buckling due to the PAN contraction. Such a stiff material restricts actuation and requires a more compliant alternative. Compliant electrodes are intended for high strain applications where conductivity must be maintained throughout. Due to the high compliance, stiffness is minimal, contributing little resistance towards actuation strains.

Wu et. al have developed flexible, transparent electrodes for solar cell applications using copper nanofiber networks (See Figure 48). Electrospun copper nanofibers are shown to have low junction resistance across contact points. Cu nanofibers produced a sheet resistance of $11 \times 10^{-3} \Omega^{-1}$, outperforming other transparent electrodes [52]. The benefit of metal nanofiber networks is the improved strain capabilities in comparison to continuous copper films. Strains up to 10% were applied within little degradation in performance.

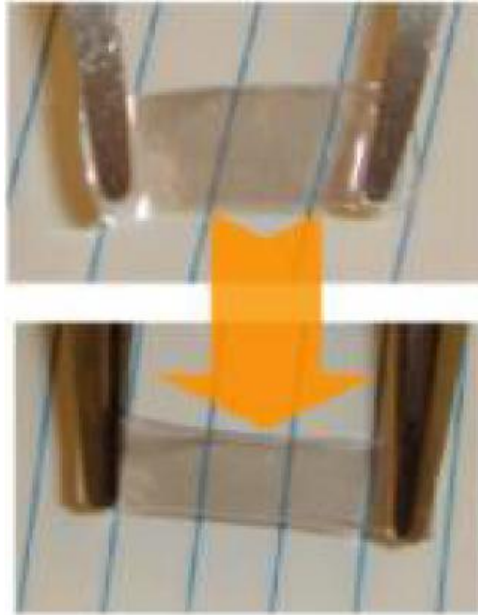


Figure 48: Transparent Cu nanofiber network under strain [52]

5.3: PAN Nanofiber Mat Properties

Response times and elongation rates of Prototype II is a significant improvement to previous works. Schreyer reported the highest rate of contraction was 27% in 10 minutes using 6.4 μm diameters PAN fibers intertwined with graphite [51]. Experimental results show a rate of contraction of 25% in 1 minute using PAN nanofibers with an average diameter of 450 nm. Reduced fiber diameter as well as the composite design contributed to better response to produced H^+ ions. A summary of PAN actuator properties is provided in Table 8.

Although the response was improved nearly ten-fold, it is far from competing with the 2 msec latency period and 10-100 msec contraction period observed in muscles [10]. As predicted by Equation 1, smaller fiber diameters increases diffusion rates and improves reaction times. Fibers as small as 5 nm have been produced through electrospinning and should be considered [36]. Careful regulation and control of electrospinning parameters will be necessary for fiber production.

Table 8: Summary of PAN fiber actuators in comparison to natural muscle

| Summary of Electrochemical PAN Actuation properties | | | |
|--|---------------------|-------------------|--------------|
| Property | Natural Muscle [13] | PAN Fiber [51] | Current Work |
| Fiber Diameter | - | 7.0 μm | 470 nm |
| Strain (%) | >40 | 27 | 58.8 |
| Stress (MPa) | 0.35 | 1.5, 5.0* | 0.08, 77.1* |
| Density kg/m ³ | 1037 | - | 0.04 (dry) |
| Strain Rate | >50 %/sec | 2.7 %/min | 25%/min |
| Cycle Life | >10e9 | - | - |
| Modulus (MPa) | 10-60 | 1.0-3.9 | 0.207 |

*Elongated State, Contracted State

Data collected from chemical and electrochemical actuation shown similar % changes in length and width. The random orientation of collected nanofibers creates a uniform reduction in area during contraction. Since activated PAN nanofibers have the greatest volume change in the axial direction, it is preferred to orient fibers in the same direction to emphasize contraction in a linear fashion [51]. The use of a rotating spindle during electrospinning orients the nanofibers along its circumference. Aligned fibers will also improve Young's Modulus of the material.

Chapter 6: Conclusion

The application of biomimetics on sarcomeres and myofibril function provided inspiration to copy certain characteristics and functionalities for artificial muscle actuators. The use of electrospun PAN nanofiber mats for actuation is analogous to the nanoscale actin and myosin filaments responsible for sarcomere contraction. The production of ions from electrolysis necessary to actuate activated PAN can be modeled from the controlled release of Ca^{+2} from SR membranes to initiate contraction. Even distribution of capillaries throughout muscle tissue served as a design concept to improve ion transport and solution diffusion throughout the PAN nanofiber networks. Unlike most EAPs used for actuation, the PAN-base actuators developed contract on a very similar basis as skeletal muscles do where as EAPs typically expand.

MWCNTs and Graphite nanofibers were introduced to the polymeric solution used for the electrospinning process. The produced PAN nanofiber composites then followed the same activation process. The composite nanofiber mats did not maintain structural integrity and became too amorphous to handle properly. The mechanical properties of composite nanofiber mats significantly decrease upon activation. Additionally, any increases in conduction were not significant enough to operate the PAN nanofiber composite as an electrode. Combining the resulting amorphous structure with the poor conductivity dissuades the concept of integrating conductive material to create an actuating nanofiber composite. Although this objective was not met, an electrolysis based actuator for PAN nanofibers was still sought after by resorting to alternative electrode materials.

Various testing was conducted to address some of the inhibiting factors of PAN fiber actuation performance. Changes of pH local to the electrode surface over time were observed at voltages ranging 5-15V. As voltage increases, water rapidly decomposes, producing high

concentrations of H^+ ions at the anode for contraction and OH^- ions at the cathode for elongation. The immediate increase or decrease of pH far exceeds pH thresholds necessary for elongation and contraction, respectively.

The effects of annealing times on mechanical properties for dry and activated PAN nanofiber mats were observed through tensile testing. Of the three materials, the activated PAN nanofibers in the expanded state had the lowest stiffness and strength. The contracted state however, had the greatest ultimate strength and maximum strain. The contraction capabilities reduced as annealing time increased, due to lowered availability of carboxyl ions for actuation. The largest achieved ultimate stress, contractile strain, and young's modulus from the tensile testing was 77.1 MPa, 58.8%, and 0.207 MPa, respectively. With the exception of the young's modulus, the mechanical properties surpass the necessary requirements for muscle properties. The best overall performance can be found for samples annealed at 2.5 hours.

PAN/ Graphite Sheet Composite actuators were fabricated and tested for contraction and elongation rates. Contact area is crucial to maximize diffusion rates and exposure of produced ions. Contraction rates up to 25%/min were observed. The results showed significant improvements over previous work done, but requires additional work to obtain contraction rates similar to muscle. Research into the diffusion characteristics of the material, taking full advantage of the nanoscale material properties, and finding methods to speed up the reaction rates of the electrolysis process is necessary to advance PAN-based actuators to performance levels similar to natural muscle. Investigations into corrosion resistant compliant electrodes are recommended to consider use of PAN nanofibers for high performance actuation.

Chapter 7: Future Work

The following recommendations are provided for future investigations towards improving the design and functionality of PAN composite actuators:

1. Create aligned PAN nanofiber mats to take advantage of the unidirectional mechanical properties in the axial direction to improve stiffness of the material as well as maximize contraction strain.
2. Successfully produce PAN nanofibers through electrospinning or through other means with diameters below 100 nm to take advantage of the high diffusion rates across smaller diameter polymer chains and increase contraction and elongation rates of the material.
3. Integrate compliant inert electrode materials with PAN nanofibers to withstand dynamic and corrosive environments for improved cyclic performance and material properties.
4. Use alternative electrolytic solution for electrolysis to prevent the formation of byproducts that may degrade the actuation performance of the PAN composite over time.
5. Measure force capacity of future PAN nanofiber-based prototypes designed for electrochemical actuation to characterize dynamic performance
6. Develop a model to simulate the electrochemomechanical response of the PAN nanofiber composites within electrolytic solution to predict the influence of multiple design and processing parameters on actuation performance.

References:

- [1] "Biomimetics." Biomimetics - Definition and More from the Free Merriam-Webster Dictionary. N.p., n.d. Web.
- [2] "Flying Machine." Leonardo Da Vinci's Flying Machine Invention. N.p., n.d. Web. 16 Apr. 2013.
- [3] "Design Heroes: Fiona Fairhurst." BBC News. BBC, 05 Aug. 2009. Web. 16 Apr. 2013.
- [4] "Self-Cleaning Materials: Lotus Leaf-Inspired Nanotechnology: Scientific American." Self-Cleaning Materials: Lotus Leaf-Inspired Nanotechnology: Scientific American. N.p., n.d. Web. 17 Apr. 2013.
- [5] Rachmuth, Guy, Harel Z. Shouval, Mark F. Bear, and Chi-Sang Poon. "A Biophysically-based Neuromorphic Model of Spike Rate- and Timing-dependent Plasticity." Ed. Leon N. Cooper. *A Biophysically-based Neuromorphic Model of Spike Rate- and Timing-dependent Plasticity* (2011): n. pag. Print.
- [6] Organovo. N.p., n.d. Web. 17 Apr. 2013.
- [7] Leonardo da Vinci: ornithopter. Photograph. Encyclopædia Britannica Online. Web. 17 Apr. 2013. <<http://www.britannica.com/EBchecked/media/95182/Leonardo-da-Vincis-plans-for-an-ornithopter-a-flying-machine>>
- [8] Hunter, Ian W., and Serge Lafontaine. "A Comparison of Muscle with Artificial Actuators." *IEEE* (1992): 178-85. Print.
- [9] Colbourne, Helen. *Inquiry into Biology*. Toronto: McGraw-Hill Ryerson, 2007. 335. Print.
- [10] Shahinpoor, Mohsen, Kwang J. Kim, and Mehran Mojarad. *Artificial Muscles: Applications of Advanced Polymeric Nanocomposites*. New York: Taylor & Francis, 2007. Print.
- [11] Herzog, W. *Skeletal Muscle Mechanics: From Mechanisms to Function*. Chichester: Wiley, 2000. Print.
- [12] Lodish, Harvey F. "Figure 17-30." *Molecular Cell Biology*. New York: W.H. Freeman, 2008. N. pag. Print.
- [13] Madden, J.D.W., N.A. Vandesteeg, P.A. Anquetil, P.G.A. Madden, A. Takshi, R.Z. Pytel, S.R. Lafontaine, P.A. Wieringa, and I.W. Hunter. "Artificial Muscle Technology: Physical Principles and Naval Prospects." *IEEE Journal of Oceanic Engineering* 29.3 (2004): 706-28. Print.

- [14] Lee, D., Y. Kim, S. Lee, M. Lee, J. Lee, B. Kim, and N. Cho. "Characteristics of Chemo-mechanically Driven Polyacrylonitrile Fiber Gel Actuators." *Materials Science and Engineering: C* 28.2 (2008): 294-98. Print.
- [15] "UBC ECE | Electrical and Computer Engineering | UBC" from http://www.ece.ubc.ca/~tissa/accedu_files/diel_compression.jpg
- [16] Kovacs, G., 2009, "Contractive Tension Force Stack Actuator Based on Soft Dielectric Eap," *Proc. SPIE*, 7287(1), pp. 72870A.
- [17] Biddiss, E., and Chau, T., 2008, "Dielectric Elastomers as Actuators for Upper Limb Prosthetics: Challenges and Opportunities," *Medical Engineering & Physics*, 30(4), pp. 403-418.
- [18] "Ionic Polymer-Metal Composite:." *Smart Structures*. N.p., n.d. Web. 02 May 2013.
- [19] Shahinpoor, M., Y. Bar-Cohen, J. O. Simpson, and J. Smith. "Ionic Polymer-metal Composites (IPMCs) as Biomimetic Sensors, Actuators and Artificial Muscles - a Review." *Smart Materials and Structures* 7.6 (1998): R15-30. Print.
- [20] Martinez, José G., Joaquín Arias-Pardilla, and Toribio F. Otero. "Simultaneous Smart Actuating-Sensing Devices Based on Conducting Polymers." *InTech* (2012): 283-310. Print.
- [21] Madden, J. D. "Polypyrrole Actuators: Properties and Initial Applications." (n.d.): 122-52. Print.
- [22] Maton, Anthea. *Human Biology and Health*. Englewood Cliffs, NJ: Prentice Hall, 1993. Print.
- [23] Polyacrylonitrile." *Polyacrylonitrile*. N.p., n.d. Web. 20 Apr. 2013.
- [24] "Innovation Starts Here." *DuPont Heritage Timeline*. N.p., n.d. Web. 20 Apr. 2013.
- [25] Yusof, N., and A. F. Ismail. "Post Spinning and Pyrolysis Processes of Polyacrylonitrile (PAN) - Based Carbon Fiber and Activated Carbon Fiber: A Review." *Journal of Analytical and Applied Pyrolysis* 93 (2011): n. pag. Print.
- [26] Shahinpoor, M., Kim, K. J., and Schreyer, H. B., 2000, "Artificial Sarcomere and Muscle Made with Conductive Polyacrylonitrile (C-Pan) Fiber Bundles," *Proceedings of the SPIE - The International Society for Optical Engineering*, 3987(pp. 243-51.
- [27] Rosenbaum, Shlomo. "Polyacrylonitrile Fiber Behavior." *Journal of Applied Polymer Science* 9 (1965): 2071-084. Print.

- [28] "Omnexus Accelerates Technology and Business Development with Plastics & Elastomers." Omnexus Accelerates Technology and Business Development with Plastics & Elastomers. N.p., n.d. Web. 20 Apr. 2013.
- [29] Umemoto, S., T. Matsumura, T. Sakai, and N. Okui. "Elongation/contraction Properties for Poly(acrylonitrile) Gel Fibers Stimulated by PH." *Polymer Gels and Networks* 1.2 (1993): 115-26.
- [30] Choe, K. "Performance Characteristics of Electro-chemically Driven Polyacrylonitrile Fiber Bundle Actuators." *Journal of Intelligent Material Systems and Structures* 17.7 (2006): 563-76. Print.
- [31] Gatford, Joanna. A diagram of the electrospinning process showing the onset of instability. Digital image. The New Zealand Institute for Plant and Food Research Ltd, 8 Sept. 2008. Web.
- [32] Naraghi, M., Chasiotis, Ioannis, 2010, "Mechanics of Pan Nanofibers," Springer Netherlands.
- [33] Naraghi, M., S.n. Arshad, and I. Chasiotis. "Molecular Orientation and Mechanical Property Size Effects in Electrospun Polyacrylonitrile Nanofibers." *Polymer* (2011): n. pag. Print.
- [34] Abuzade, Ramazan Ali, Ali Zadhoush, and Ali Akbar Gharehaghaji. "Air Permeability of Electrospun Polyacrylonitrile Nanoweb." *Journal of Applied Polymer Science* (2012): 232-43. Print.
- [35] Wang, Tong, and Satish Kumar. "Electrospinning of Polyacrylonitrile Nanofibers." *Journal of Applied Polymer Science* (2005): 1023-029. Print.
- [36] Tan, S-H., R. Inai, M. Kotaki, and S. Ramakrishna. "Systematic Parameter Study for Ultra-fine Fiber Fabrication via Electrospinning Process." *Polymer* 46.16 (2005): 6128-134. Print.
- [37] Huang, Zheng-Ming, Y.-Z. Zhang, M. Kotaki, and S. Ramakrishna. "A Review on Polymer Nanofibers by Electrospinning and Their Applications in Nanocomposites." *Composites Science and Technology* (2003): 2223-253. Print.
- [38] Kim, J., S. Choi, S. Jo, W. Lee, and B. Kim. "Electrospun PVdF-based Fibrous Polymer Electrolytes for Lithium Ion Polymer Batteries." *Electrochimica Acta* 50.1 (2004): 69-75. Print.

- [39] Gu, S. Y., J. Ren, and G. J. Vancso. "Process Optimization and Empirical Modeling for Electrospun Polyacrylonitrile (PAN) Nanofiber Precursor of Carbon Nanofibers." *European Polymer Journal* (2005): 2559-568. Print.
- [40] Gou, Z. "Two-dimensional Modeling of Dry Spinning of Polymer Fibers." *Journal of Non-Newtonian Fluid Mechanics* 118.2-3 (2004): 121-36. Print.
- [41] Ramakrishna, Seeram. *An Introduction to Electrospinning and Nanofibers*. Singapore: World Scientific, 2005. Print.
- [42] Gestos, Adrian, Philip G. Whitten, Gordon G. Wallace, and Geoffrey M. Spinks. "Actuating Individual Electrospun Hydrogel Nanofibres." (2012): 8082-087. Print.
- [43] Samatham, R., K. Choe, K. J. Kim, M. Shahinpoor, and J. D. Nam. "Towards Nano-biomimetic Muscles: Polyacrylonitrile Nanofibers." *Smart Structures and Materials* (2004): 235-41. Print.
- [44] Samatham, R., I-S Park, K. J. Kim, J-D Nam, N. Whisman, and J. Adams. "Electrospun Nanoscale Polyacrylonitrile Artificial Muscle." *Smart Materials and Structures* 15.6 (2006): N152-156. Print.
- [45] Deruiter, Jack. "Carboxylic Acid Structure and Chemistry: Part 1." *Principles of Drug Action 1*, Spring 2005, Carboxylic Acids Part 1. N.p., n.d. Web.
- [46] Bin, He, Liu Sha, Li Yonggang, and Wang Kun. "Research of PH Gradient on Swimming Bacteria Control." *IEEE* (2010): 1004-007. Print.
- [47] Almuhammed, Silman, Nabyl Khenoussi, Laurence Schacher, Dominique Adolphe, and Henri Balard. "Measuring of Electrical Properties of MWNT - Reinforced PAN Nanocomposites." *Journal of Nanomaterials* 2012 (2012): n. pag. Web.

- [48] Ge, Jason J., Haoqing Hou, Qing Li, Matthew J. Graham, Andreas Greiner, Darrell H. Reneker, Frank W. Harris, and Stephen Z.D. Cheng. "Assembly of Well-aligned Multiwalled Carbon Nanotubes in Confined Polyacrylonitrile Environments: Electrospun Composite Nanofiber Sheets." American Chemical Society (2004): 15754-5761. Web.
- [49] Fraczek, A., and S. Blazewicz. "Effects of Dispersion of Carbon Nanotubes in Polyacrylonitrile Matrix on Mechanical and Thermal Behavior of Nanocomposites." Journal of Physics (2009): n. pag. Web.
- [50] Serway, Raymond A. Principles of Physics. Fort Worth: Saunders College Pub., 1998. Print.
- [51] Schreyer, H. Brett, Nouvelle Gebhart, Kwang J. Kim, and Mohsen Shahinpoor. "Electrical Activation of Artificial Muscles Containing Polyacrylonitrile Gel Fibers." Biomacromolecules 1.4 (2000): 642-47. Print.
- [52] Wu, Hui, Liangbing Hu, Michael W. Rowell, Desheng Kong, Judy J. Cha, James R. McDonough, Jia Zhu, Yuan Yang, Michael D. McGehee, and Yi Cui. "Electrospun Metal Nanofiber Webs as High Performance Transparent Electrode." American Chemical Society (2010): 4242-248. Web.

Appendix A: Characteristics and Challenges of Dielectric Elastomers [17]

Table 4
Summary of current challenges limiting the use of DE actuators in upper extremity prosthetics and opportunities for future development

| Actuator characteristics | Challenges | Areas for future development |
|---|--|---|
| Durability | | |
| Multiple failure mechanisms | Limits reliability and performance to a narrow operating range | Development of DEs with higher moduli of elasticity (to prevent material strength failure and pull-in failure) and higher dielectric constants that operate at lower voltages (to prevent dielectric breakdown) |
| Fatigue | May potentially limit the operating life of DE actuators to an unacceptable level (i.e. $<10^6$ cycles) | Further characterization of the fatigue life of DE actuators, particularly when operating under load |
| High susceptibility to contaminants | Requires isolation of DE actuators from contaminants during manufacture and operation to prevent early failure or degraded performance | Development of encapsulation strategies is needed to protect actuators from particle and liquid contaminants |
| Inconsistent and/or challenging manufacture | Complicates characterization of actuator performance and reliability | Development of fully automated fabrication techniques |
| Precision control | | |
| Stress relaxation | Limits shelf-life of actuators and induces time dependence of performance and control | Elimination of pre-strain in actuator design |
| Creep | Limits precise control during sustained actuations | Further development of theoretical models to capture and predict nonlinear material responses along with development of less viscoelastic DE materials |
| Hysteresis | Increases complexity of control systems | |
| Viscoelasticity | Induces a dependence of performance and control on operating speed | |
| Energy consumption | | |
| Efficiency | Decreases with operating frequency | Reduction of viscoelastic losses that lead to poor efficiency at high speeds |
| Power density | Increases with operating frequency | |
| Current leakage | Limits reliable actuation at low speeds or for continuous operation | Miniaturization of high voltage conversion and recovery circuitry |
| Electromechanical efficiency | Limits attainable energy efficiency | |
| High voltages | Requires high voltage dc conversion, recovery and current limiting circuitry that reduces actuation speed and increases system complexity and bulk Introduces possible risk of shock and related consumer safety concerns | Development of thin-layer DEs with higher dielectric constants for reduced voltage requirements Development and testing of strategies to isolate the user from high voltages |
| Anthropomorphism | | |
| Size and weight | Unacceptable size and weight for upper limb prosthetic applications | Elimination of passive and pre-straining structures that reduce size and weight efficiency |
| Force generation | Insufficient force generation at typical operating speeds | Use of parallel actuator arrays to boost force generation |
| Linear actuation and strain | Current strain performance requires long actuator lengths | Development of DE actuators with increased strain response to reduce the length of actuator required Design of actuator configurations (i.e. coils, bending) that can be efficiently packaged in a terminal device |

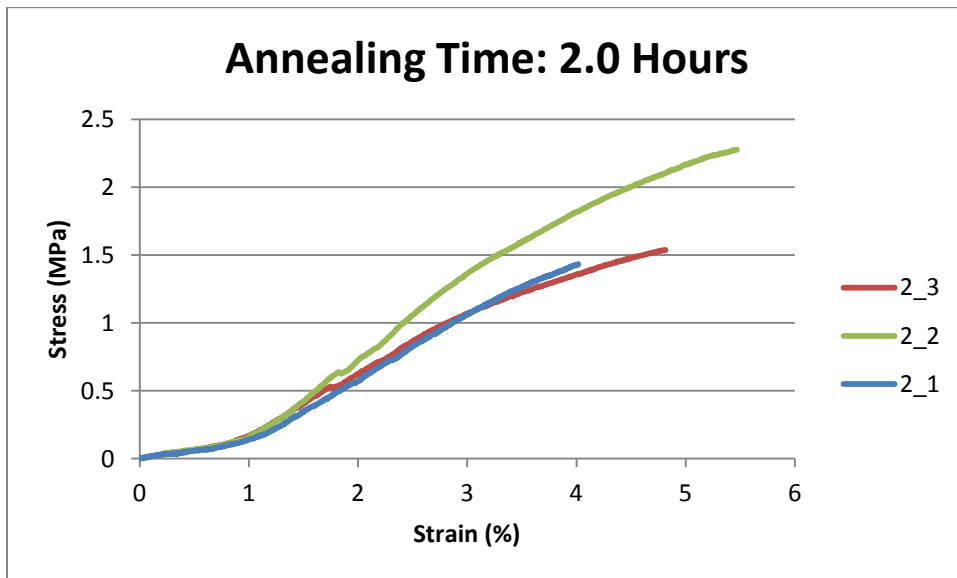
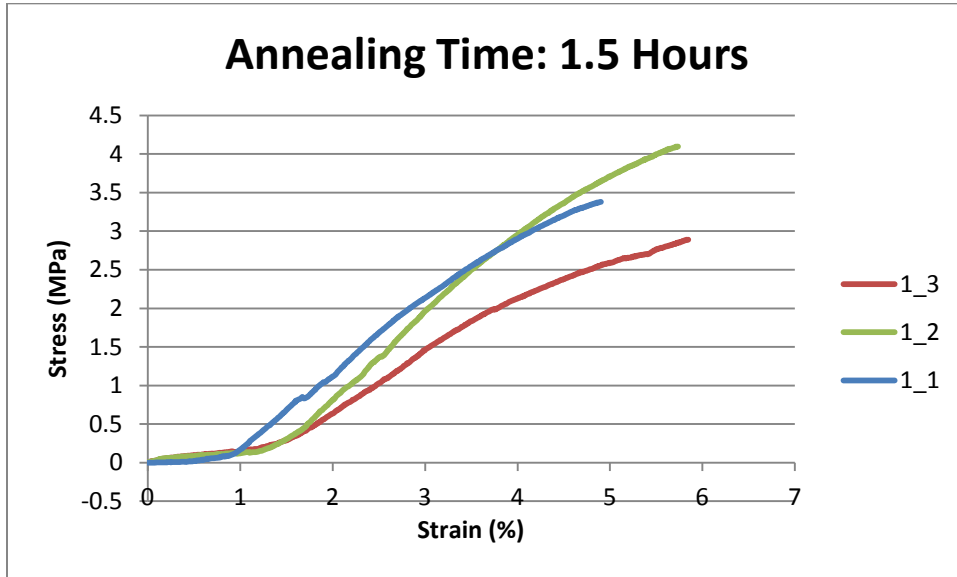
Appendix B: Summary of Current Actuator Properties [13]

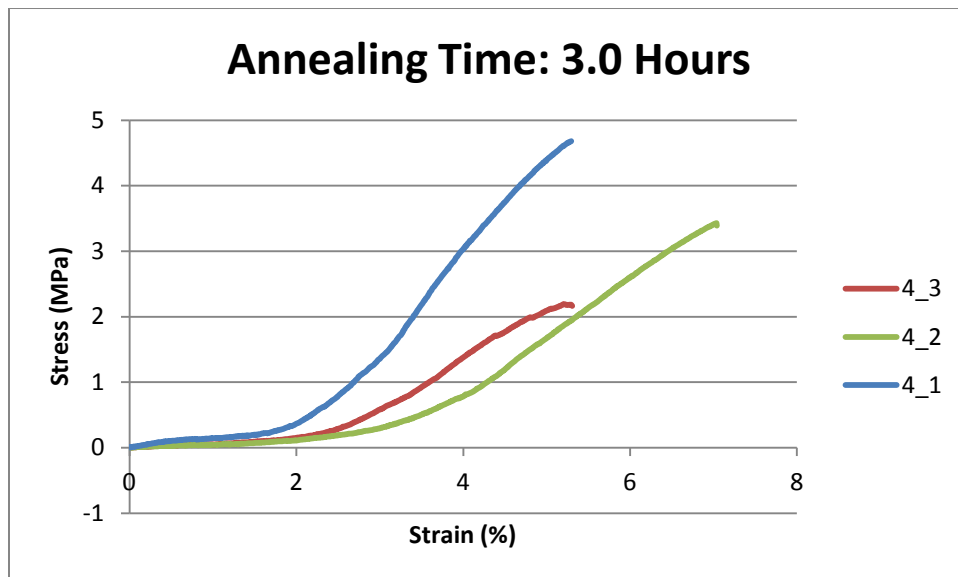
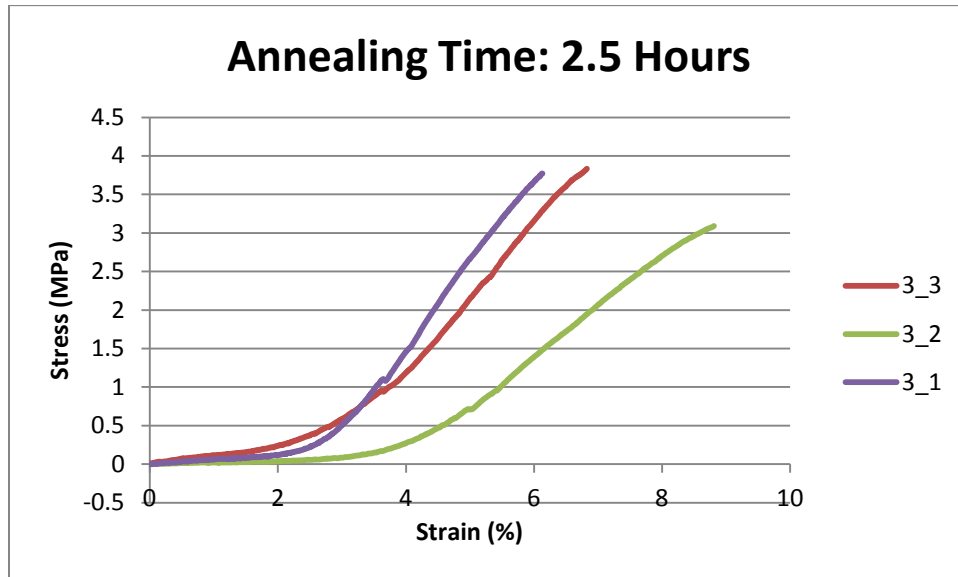
TABLE XII
ACTUATOR SUMMARY

| Actuator | Advantages | Disadvantages | Comments |
|---|--|--|--|
| Mammalian Skeletal Muscle | Large strains (20 %). Moderate Stress (350 kPa blocking). Variable stiffness. High energy fuel (20-40 MJ/kg). Efficient (~40 %). Good work density (< 40 kJ/kg). High cycle life (by regeneration). | Not yet an engineering material. Narrow temperature range of operation. No catch state (expends energy to maintain a force w/o moving, unlike mollusk muscle). | Incredibly elegant mechanism that is a challenge to emulate. Muscle is a 3D nanofabricated system with integrated sensors, energy delivery, waste/heat removal, local energy supply and repair mechanisms. |
| Dielectric Elastomers | Large strain (20% - 380 %). Moderate stress (several MPa peak). Large work density (10k to 3.4 MJ/m ³). Moderate to high bandwidth (10 Hz to > 1 kHz). Low cost. Low current. Good electromechanical coupling & efficiency (> 15 % typical, 90 % max). | High voltages (> 1 kV) and fields (~150 MV/m). Typically requires DC-DC converters. Compliant ($E \sim 1$ MPa). Pre-stretching mechanisms currently add substantial mass and volume, reducing actual work density and stress. | Potential to lower fields using high dielectric materials. Small devices are favored for high frequency operation eg. MEMS. (due to the more efficient heat transfer which prevents thermal degradation, and the higher resonant frequencies). Starting materials are readily available. |
| Relaxor Ferroelectric Polymers | Moderate strain (< 7 %). High stress (45 MPa blocking). Very high work density (up to 1 MJ/m ³ internal strain). Stiff (400 MPa). Strong coupling (0.4) & efficiency. Low current. | High voltages (typically > 1kV) and fields (~150 MV/m). Typically need DC-DC converters. Synthesis of typical materials involves environmentally regulated substances. Cycle life is unclear & may be limited by electrode fatigue and dissipation. Limited temperature range. | Lower voltages and fields are being achieved using new high dielectric composites. Small devices are favored for high frequency operation eg. MEMS. Unique combination of high stiffness, moderate strain & reasonable efficiency. |
| Liquid Crystal Elastomers | Large strains in thermally induced materials (45%). Moderate strains in field induced materials (2-4 %). High coupling (75%) in electrical materials. | Subject to creep. Thermal versions are slow unless very thin or photoactivated. High fields (1-25 MV/m). Low efficiency in thermal materials. | New material with much promise and much characterization to be done. Photo-activation has been achieved. |
| Conducting Polymers | High stress (34 MPa max, 5 MPa typical). Moderate strain (~2 %). Low voltage (~2 V). High work density (100 kJ/m ³). Stiff polymers (~1 GPa). | Low electromechanical coupling. Currently slow (several hertz maximum to obtain full strain). Typically needs encapsulation. | Promising for low voltage applications. Speed and power will improve dramatically at small scales. |
| Molecular Actuators | Large strain (20 %). Moderate to high stress (> 1 MPa). Low voltage (2 V). High work density (> 100 kJ/m ³) | Currently slow. Need encapsulation. | Great promise of overcoming many of the shortcomings of conducting polymer actuators, but still very early in development. |
| Carbon Nanotubes | High stress (> 10 MPa). Low voltage (2 V). Very large operating temperature range. | Small strain (0.2 % typical). Currently has low coupling. Materials are presently expensive. | Great potential as bulk materials approach properties of individual nanotubes. |
| Ionic Polymer Metal Composites (IPMC) | Low Voltage (< 10 V). Large displacement (mechanical amplification built into the structure). | Low coupling and efficiency. Usually no catch state (consumes energy in holding a position). Requires encapsulation. | IPMC driven toys and demonstration kits are available. |
| Thermally Activated Shape Memory Alloys | Very high stress (200 MPa). Unmatched specific power (> 100 kW/kg). Moderate to large strain (1-8 %). Low voltage (actual voltage depends on wiring). Great work density (> 1 MJ/m ³) | Difficult to control (usually run between fully contracted and fully extended but not between). Large currents and low efficiencies (<5%). Cycle life is very short at large strain amplitudes. | Readily available. Generally thought of as slow, but can achieve millisecond response times using short high current pulses and water cooling. |
| Ferromagnetic Shape Memory Alloys | High stress (< 9 MPa). High frequency (> 100 Hz). Moderate strain (up to 10%). High coupling (75%). | Bulky magnets are required which greatly reduce the work density. Costly single crystal materials. | Operates in compression and thus needs a restoring force. Displacement is typically all or nothing, as intermediate states are difficult to reach reproducibly. Commercially available. |

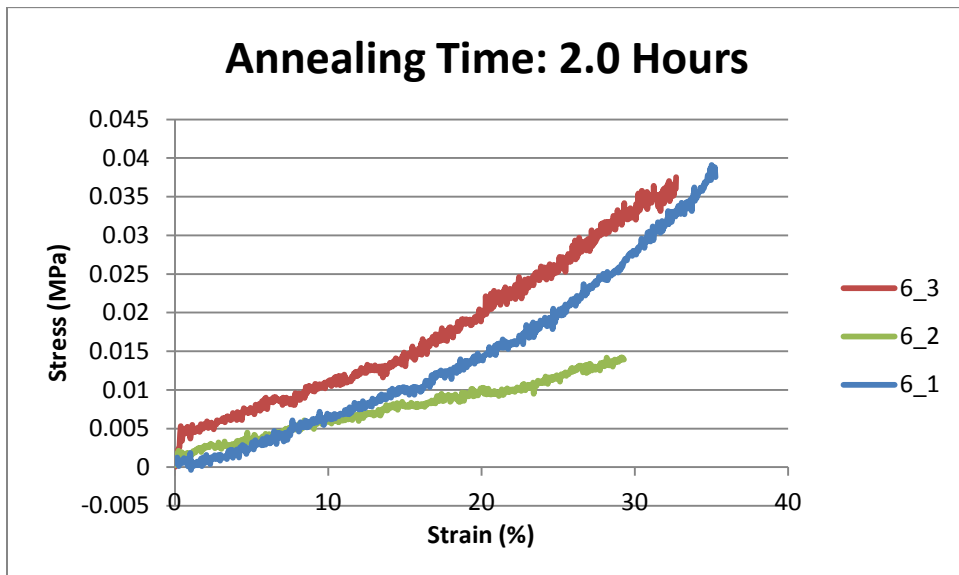
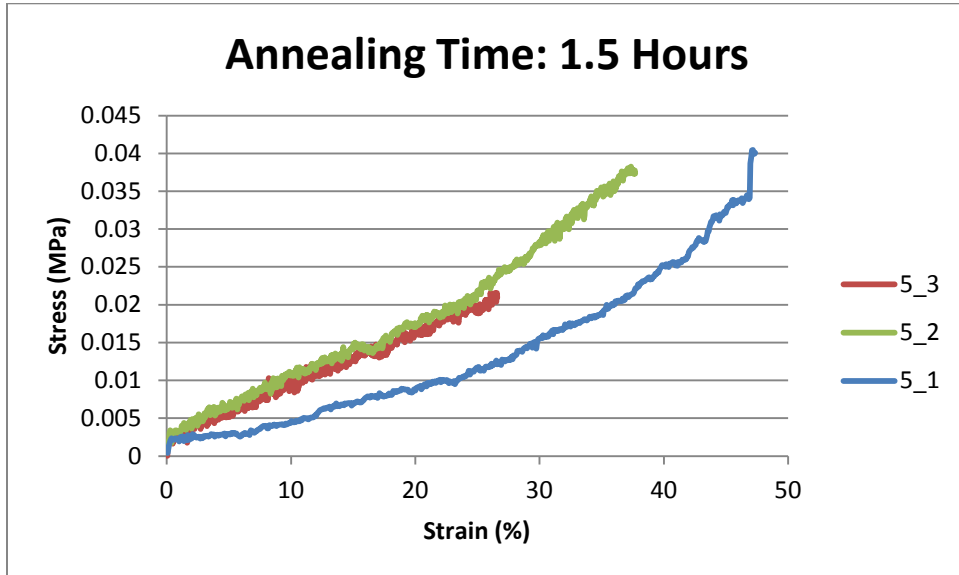
Appendix C: Tensile Testing Data

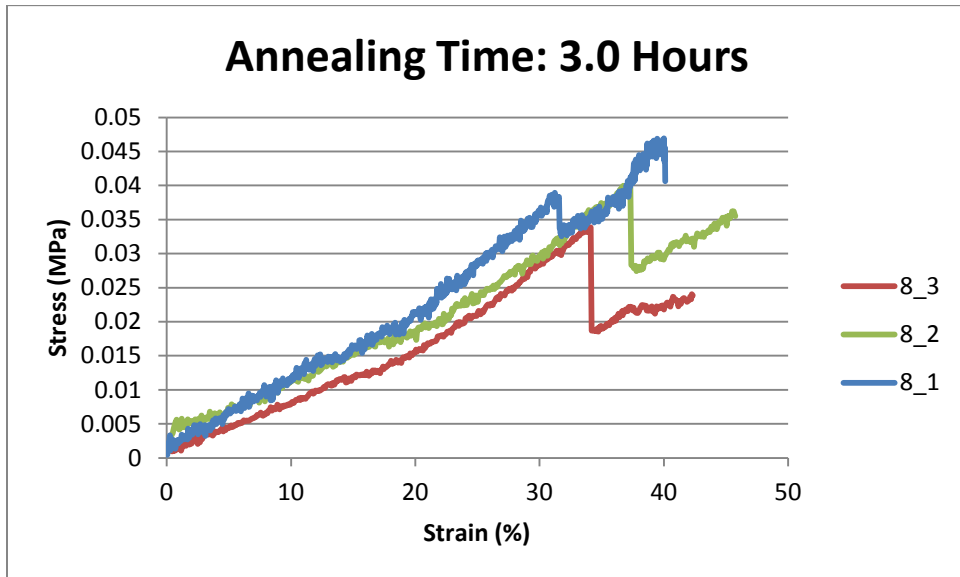
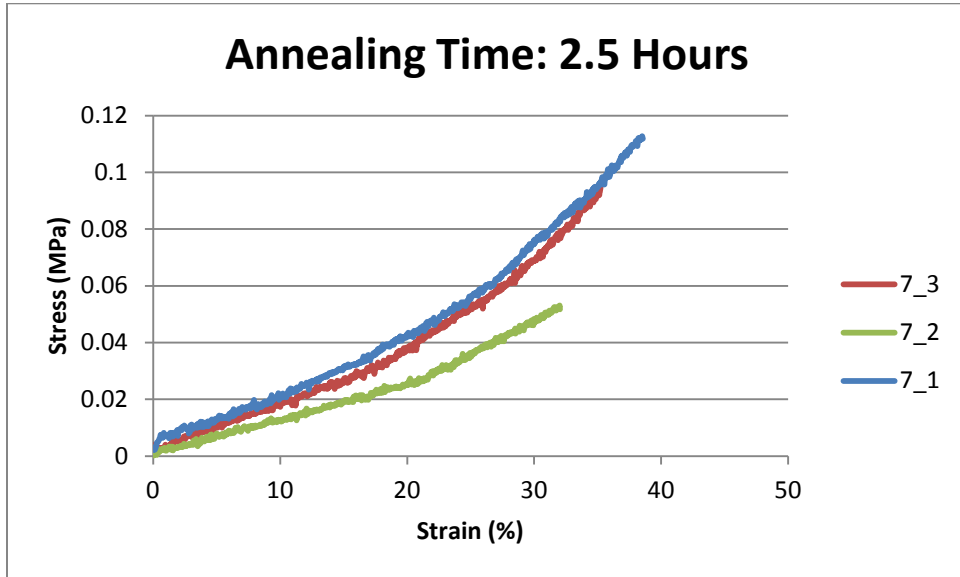
C.1: Dry PAN Nanofiber Samples



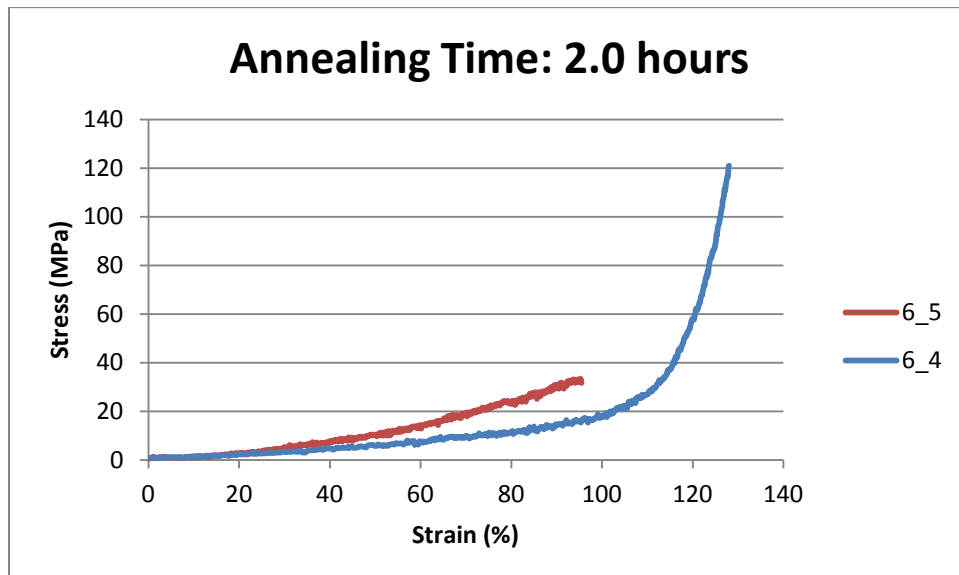
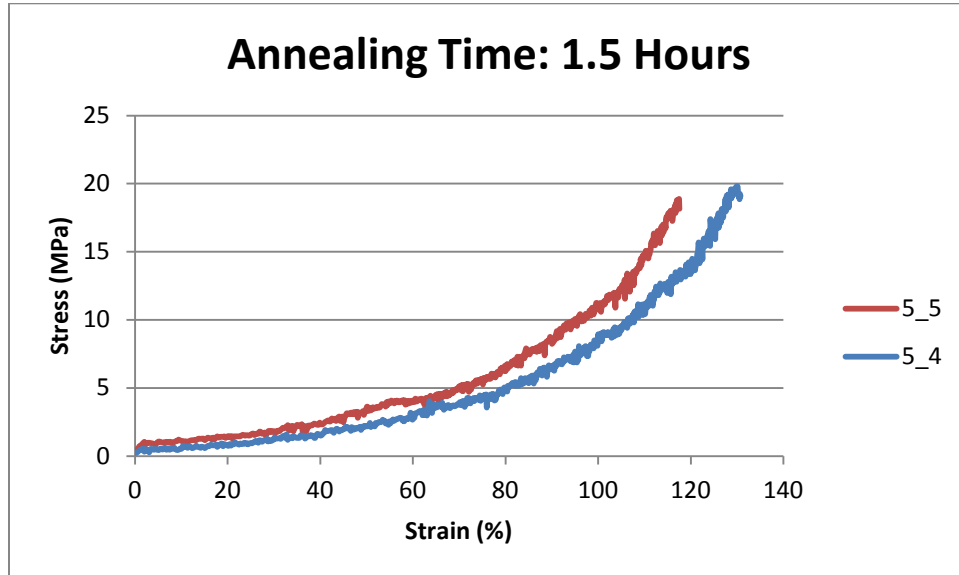


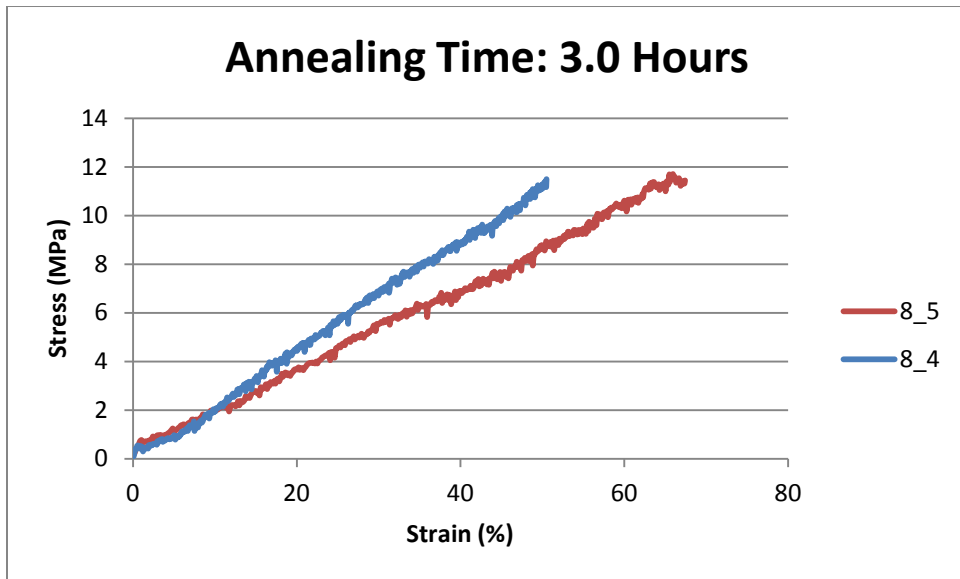
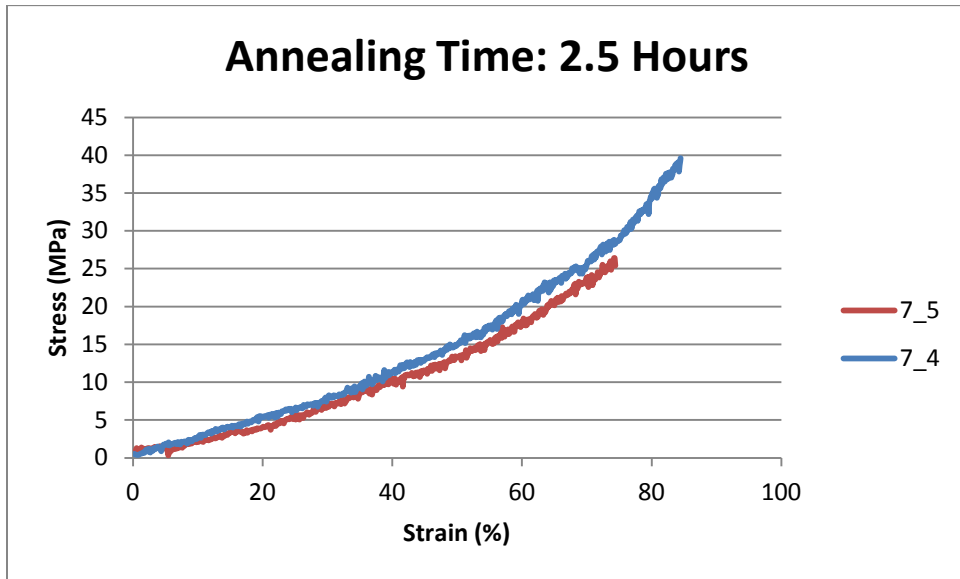
C.2: Wet Expanded PAN Nanofiber Samples





C.3: Wet Contracted PAN Nanofiber Samples





Appendix D: Panasonic “PGS” Graphite Sheets

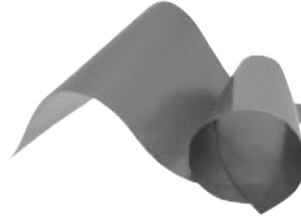
Panasonic

“PGS” Graphite Sheets

“PGS” Graphite Sheets

Type: **EYG**

PGS (Pyrolytic Graphite Sheet) is a thermal interface material which is very thin, synthetically made, has high thermal conductivity, and is made from a highly oriented graphite polymer film. It is ideal for providing thermal management/heat-sinking in limited spaces or to provide supplemental heat-sinking in addition to conventional means. This material is flexible and can be cut into customizable shapes.



■ Features

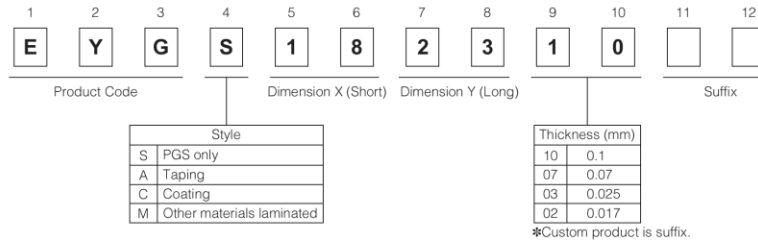
- Excellent thermal conductivity : 700 to 1750 W/(m·K)
(2 to 4 times as high as copper, 3 to 7 times as high as aluminum)
- Lightweight: Specific gravity : 0.85 to 2.1 g/cm³
(1/4 to 1/10 of copper, 1/1.3 to 1/3 of aluminum in density)
- Flexible and easy to be cut or trimmed.
(withstands repeated bending)
- Low thermal resistance
- RoHS compliant

■ Recommended applications

- Smart phones, Cellular phones, DVC, DSC, PCs and peripherals, pickup
- Semiconductor manufacturing equipment (Sputtering, Dry etching, Steppers)
- Optical communications equipment

■ Handling Precautions (Please see Page 380)

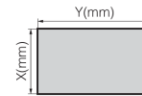
■ Explanation of Part Numbers



■ Dimensions in mm (not to scale)

Dimension of representative

| Part No. | Dimension X (Short)* | Dimension Y (Long)* | Thickness (mm) |
|--|----------------------|---------------------|--|
| EYGS1823 ¹⁰ / ₀₇ | 180±5 mm | 230±5 mm | 0.10±0.03, 0.07±0.015 |
| EYGS1218 ¹⁰ / ₀₇ ⁰³ / ₀₂ | 115±5 mm | 180±5 mm | 0.10±0.03, 0.07±0.015, 0.025±0.010, 0.017±0.005 |
| EYGS0912 ¹⁰ / ₀₇ ⁰³ / ₀₂ | 90±5 mm | 115±5 mm | 0.10±0.03, 0.07±0.015, 0.025±0.010, 0.017±0.005 |



*Please contact us for other dimensions other than those above.

Design and specifications are each subject to change without notice. Ask factory for the current technical specifications before purchase and/or use. Should a safety concern arise regarding this product, please be sure to contact us immediately.

Panasonic

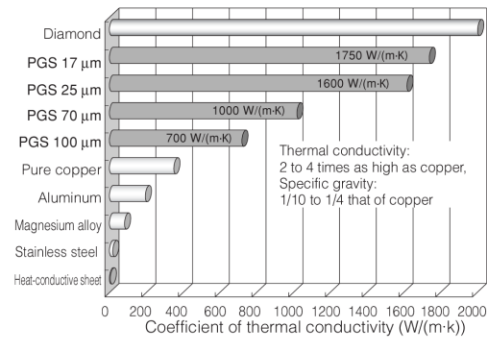
“PGS” Graphite Sheets

■ Characteristics

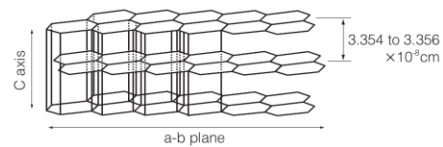
| Thickness | | 100 μm | 70 μm | 25 μm | 17 μm |
|-------------------------|-----------|--------------------------|--------------------------|--------------------------|--------------------------|
| | | 0.10 ± 0.03 mm | 0.07 ± 0.015 mm | 0.025 ± 0.010 mm | 0.017 ± 0.005 mm |
| Density | | 0.85 g/cm ³ | 1.21 g/cm ³ | 1.90 g/cm ³ | 2.10 g/cm ³ |
| Thermal conductivity | a-b plane | 700 W/(m·K) | 1000 W/(m·K) | 1600 W/(m·K) | 1750 W/(m·K) |
| Electrical conductivity | | 10000 S/cm | 10000 S/cm | 20000 S/cm | 20000 S/cm |
| Extensional strength | | 19.6 MPa | 22.0 MPa | 30.0 MPa | 40.0 MPa |
| Expansion coefficient | a-b plane | 9.3×10^{-7} 1/K | 9.3×10^{-7} 1/K | 9.3×10^{-7} 1/K | 9.3×10^{-7} 1/K |
| | c axis | 3.2×10^{-5} 1/K | 3.2×10^{-5} 1/K | 3.2×10^{-5} 1/K | 3.2×10^{-5} 1/K |
| Heat resistance | | 400 °C | | | |
| Bending(angle 180,R5) | | 10000 cycles | | | |

*Values are for reference, not guaranteed.

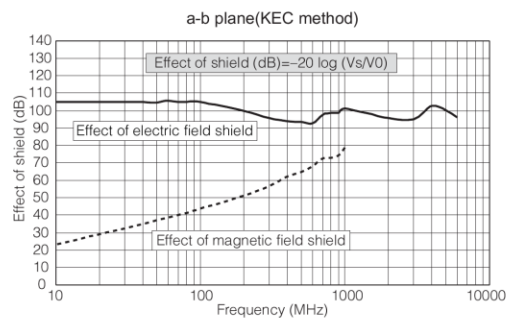
■ Comparison of thermal conductivity (a-b plane)



■ Layered structure of PGS



■ Electric field shield performance



Design and specifications are each subject to change without notice. Ask factory for the current technical specifications before purchase and/or use. Should a safety concern arise regarding this product, please be sure to contact us immediately.


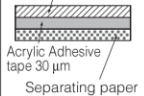
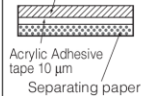
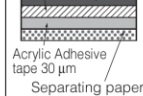
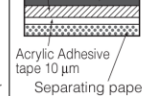
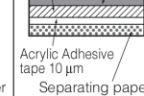
01 Nov. 2011

Panasonic

“PGS” Graphite Sheets

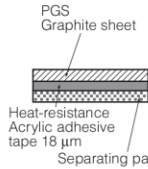
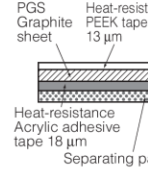
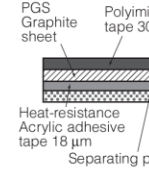
■ Rating and Characteristics

● Standard series (PGS 100, 70, 25, 17 μm)

| Type | PGS Only | Adhesive Type | | | Laminated type (Insulation & Adhesive) | | |
|-----------------------|---|---|---|--|--|--|--|
| | S type | A-A type | A-M type | A-PA type | A-PM type | A-DM type | |
| Front face | – | – | – | Polyester tape standard type 30 μm | Polyester tape standard type 30 μm | Polyester tape thin type 10 μm | |
| Rear face | – | Insulative adhesion type 30 μm | Insulative thin adhesion type 10 μm | Insulative adhesion type 30 μm | Insulative thin adhesion type 10 μm | Insulative thin adhesion type 10 μm | |
| Structure |  |  |  |  |  |  | |
| Features | ·High Thermal Conductivity ·High Flexibility ·Low Thermal Resistance ·Available up to 400 °C ·Conductive Material | ·With insulation material on one side ·With strong adhesive tape for putting chassis ·Withstanding Voltage : 2 kV | ·With insulation material on one side ·Low thermal resistance comparison with A-A type ·Withstanding Voltage : 1 kV | ·With insulation material on both side ·Withstanding Voltage PET tape : 4 kV ·Adhesive Tape : 2 kV | ·With insulation material on both side ·Withstanding Voltage PET tape : 4 kV ·Adhesive Tape : 1 kV | ·With insulation material on both side ·Withstanding Voltage PET tape : 1 kV ·Adhesive Tape : 1 kV | |
| Withstand temperature | 400 °C | 100 °C | 100 °C | 100 °C | 100 °C | 100 °C | |
| Standard Size | 115 × 180 mm | 90 × 115 mm | 90 × 115 mm | 90 × 115 mm | 90 × 115 mm | 90 × 115 mm | |
| Maximum size | 180 × 230 mm 115 × 180 mm(25 μm) | 115 × 180 mm | 115 × 180 mm | 115 × 180 mm | 115 × 180 mm | 115 × 180 mm | |
| 100 μm | Part No. EYGS121810 | – | – | – | – | – | |
| Thickness | 100 μm | – | – | – | – | – | |
| 70 μm | Part No. EYGS121807 | EYGA091207A | EYGA091207M | EYGA091207PA | EYGA091207PM | EYGA091207DM | |
| Thickness | 70 μm | 100 μm | 80 μm | 130 μm | 110 μm | 90 μm | |
| 25 μm | Part No. EYGS121803 | EYGA091203A | EYGA091203M | EYGA091203PA | EYGA091203PM | EYGA091203DM | |
| Thickness | 25 μm | 55 μm | 35 μm | 85 μm | 65 μm | 45 μm | |
| 17 μm | Part No. – | EYGA091202A | EYGA091202M | EYGA091202PA | EYGA091202PM | EYGA091202DM | |
| Thickness | – | 47 μm | 27 μm | 77 μm | 57 μm | 37 μm | |

* Please contact our engineering section or factory about to special applications.

● High heat resistance series (PGS 70, 25, 17 μm)

| Type | high heat resistance type | | |
|-----------------------|--|--|--|
| | A-V type | A-RV type | A-KV type |
| Front face | – | high heat resistance and insulation type 13 μm | high heat resistance and insulation type 30 μm |
| Rear face | High heat resistance and insulation adhesion type 18 μm | High heat resistance and insulation adhesion type 18 μm | High heat resistance and insulation adhesion type 18 μm |
| Structure |  |  |  |
| Features | ·With high heat resistance and insulation tape on one side ·Withstanding Voltage Adhesive tape : 2 kV | ·With high heat resistance and insulation tape on both side ·Withstanding Voltage PEEK tape : 2 kV ·Adhesive tape : 2 kV | ·With high heat resistance and more insulated tape on both side ·Withstanding Voltage PI tape : 5 kV ·Adhesive tape : 2 kV |
| Withstand temperature | 150 °C | 150 °C | 150 °C (Polyimide : 180 °C) |
| Standard Size | 90 × 115 mm | 90 × 115 mm | 90 × 115 mm |
| Maximum size | 115 × 180 mm | 115 × 180 mm | 115 × 180 mm |
| 70 μm | Part No. EYGA091207V | EYGA091207RV | EYGA091207KV |
| Thickness | 88 μm | 101 μm | 118 μm |
| 25 μm | Part No. EYGA091203V | EYGA091203RV | EYGA091203KV |
| Thickness | 43 μm | 56 μm | 73 μm |
| 17 μm | Part No. EYGA091202V | EYGA091202RV | EYGA091202KV |
| Thickness | 35 μm | 48 μm | 65 μm |

Design and specifications are each subject to change without notice. Ask factory for the current technical specifications before purchase and/or use. Should a safety concern arise regarding this product, please be sure to contact us immediately.

02 Feb. 2012

Panasonic**“PGS” Graphite Sheets****Minimum order**

| Item | Part No. | Type | Size | Minimum order |
|---|---|-------------------|-------------|---------------|
| PGS Graphite Sheet Only | S type 100 μm | EYGS091210 | 90×115 mm | 20 |
| | | EYGS121810 | 115×180 mm | 10 |
| | | EYGS182310 | 180×230 mm | 10 |
| | S type 70 μm | EYGS091207 | 90×115 mm | 20 |
| | | EYGS121807 | 115×180 mm | 10 |
| | | EYGS182307 | 180×230 mm | 10 |
| | S type 25 μm | EYGS091203 | 90×115 mm | 20 |
| | | EYGS121803 | 115×180 mm | 10 |
| | PGS 70, 25 μm Adhesive Type [Standard series] | A-A type 70 μm | EYGA091207A | 90×115 mm |
| EYGA121807A | | | 115×180 mm | 10 |
| A-A type 25 μm | | EYGA091203A | 90×115 mm | 20 |
| | | EYGA121803A | 115×180 mm | 10 |
| A-A type 17 μm | | EYGA091202A | 90×115 mm | 20 |
| | | EYGA121802A | 115×180 mm | 10 |
| A-M type 70 μm | | EYGA091207M | 90×115 mm | 20 |
| | | EYGA121807M | 115×180 mm | 10 |
| A-M type 25 μm | | EYGA091203M | 90×115 mm | 20 |
| | | EYGA121803M | 115×180 mm | 10 |
| A-M type 17 μm | | EYGA091202M | 90×115 mm | 20 |
| | | EYGA121802M | 115×180 mm | 10 |
| PGS 70, 25 μm Laminated Type (Insulation & Adhesive) [Standard series] | A-PA type 70 μm | EYGA091207PA | 90×115 mm | 20 |
| | | EYGA121807PA | 115×180 mm | 10 |
| | A-PA type 25 μm | EYGA091203PA | 90×115 mm | 20 |
| | | EYGA121803PA | 115×180 mm | 10 |
| | A-PA type 17 μm | EYGA091202PA | 90×115 mm | 20 |
| | | EYGA121802PA | 115×180 mm | 10 |
| | A-PM type 70 μm | EYGA091207PM | 90×115 mm | 20 |
| | | EYGA121807PM | 115×180 mm | 10 |
| | A-PM type 25 μm | EYGA091203PM | 90×115 mm | 20 |
| | | EYGA121803PM | 115×180 mm | 10 |
| | A-PM type 17 μm | EYGA091202PM | 90×115 mm | 20 |
| | | EYGA121802PM | 115×180 mm | 10 |
| | A-DM type 70 μm | EYGA091207DM | 90×115 mm | 20 |
| | | EYGA121807DM | 115×180 mm | 10 |
| | A-DM type 25 μm | EYGA091203DM | 90×115 mm | 20 |
| | | EYGA121803DM | 115×180 mm | 10 |
| | A-DM type 17 μm | EYGA091202DM | 90×115 mm | 20 |
| | | EYGA121802DM | 115×180 mm | 10 |
| PGS 70, 25 μm [High heat resistance type] | A-V type 70 μm | EYGA091207V | 90×115 mm | 20 |
| | | EYGA121807V | 115×180 mm | 10 |
| | A-V type 25 μm | EYGA091203V | 90×115 mm | 20 |
| | | EYGA121803V | 115×180 mm | 10 |
| | A-V type 17 μm | EYGA091202V | 90×115 mm | 20 |
| | | EYGA121802V | 115×180 mm | 10 |
| | A-RV type 70 μm | EYGA091207RV | 90×115 mm | 20 |
| | | EYGA121807RV | 115×180 mm | 10 |
| | A-RV type 25 μm | EYGA091203RV | 90×115 mm | 20 |
| | | EYGA121803RV | 115×180 mm | 10 |
| | A-RV type 17 μm | EYGA091202RV | 90×115 mm | 20 |
| | | EYGA121802RV | 115×180 mm | 10 |
| | A-KV type 70 μm | EYGA091207KV | 90×115 mm | 20 |
| | | EYGA121807KV | 115×180 mm | 10 |
| | A-KV type 25 μm | EYGA091203KV | 90×115 mm | 20 |
| | | EYGA121803KV | 115×180 mm | 10 |
| | A-KV type 17 μm | EYGA091202KV | 90×115 mm | 20 |
| | | EYGA121802KV | 115×180 mm | 10 |

** Please consult if the quantity of orders is little.

Appendix E: Sylgard® 184 Silicone Elastomer

Product Information Solar

DOW CORNING

Sylgard® 184 Silicone Elastomer

FEATURES

- Transparent
- Cures to flexible elastomer
- Constant cure rate, regardless of sectional thickness or degree of confinement
- Service range of -45 to 200°C (-49 to 392°F)
- No post cure required
- Two part, 10:1 mix
- RT/HA cure
- Minimal shrinkage
- No exotherm during cure
- No solvents or cure byproducts
- Repairable
- Good dielectric properties
- Deep section cure
- UL 94 V1, V0
- UL RTI 130°C (266°F)

COMPOSITION

- Two-part silicone elastomer supplied as flowable liquid

Two-part silicone that cures to a flexible elastomer for protection of electrical and electronic devices in solar applications

APPLICATIONS

- Protection of electrical/electronic devices.
- General potting applications including power supplies, connectors, sensors, industrial controls, transformers, amplifiers, high voltage resistor packs, and relays; adhesive/encapsulant for solar cells.

TYPICAL PROPERTIES

Specification Writers: Please contact your local Dow Corning sales office or your Global Dow Corning contact before writing specifications on this product.

| Test | Unit | Result |
|--|---------------------|------------------------|
| Mix Ratio | | 10:1 |
| Color | | Clear |
| Viscosity | centipoise or mPa.s | 3900 |
| Durometer, Shore A | | 50 |
| Specific Gravity | | 1.03 |
| Working Time at RT | min | >2 hours |
| Thermal Conductivity | Watt/meter-°K | 0.2 |
| | cal/cm-sec °C | 4.3 x 10 ⁻⁴ |
| Linear Coefficient of Thermal Expansion | µm/m-°C or ppm | 310 |
| UL Flammability Classification | | 94 V1, V0 |
| UL Temperature Index, Electrical/ Mechanical | °C | 130/130 |
| Dielectric Strength | volts/mil | 540 |
| | kV/mm | 21.2 |
| Dielectric Constant at 100 Hz | | 2.7 |
| Dielectric Constant at 100 kHz | | 2.7 |
| Volume Resistivity | ohm-cm | 1.2 x 10 ¹⁴ |
| Dissipation Factor at 100 Hz | | <0.001 |
| Dissipation Factor at 100 kHz | | <0.001 |

DESCRIPTION

Sylgard® 184 Silicone Elastomer is supplied as two-part liquid component kits comprised of Part A/Part B to be mixed in a 10:1 ratio by weight or volume. It is suitable for manual mixing or automated mixing and dispensing.

When liquid components are thoroughly mixed, the mixture cures to a flexible elastomer, which is suited for the protection of electrical/electronic devices in solar applications.

HOW TO USE

Mixing

Sylgard 184 Silicone Elastomer is supplied in two parts as lot-matched base and curing agent that are mixed in a ratio of 10 parts base to one part curing agent, by weight. For further information, consult your local Dow Corning representative.

Pot Life/Working Time

Cure reaction begins with the mixing process. Initially, cure is evidenced by a gradual increase in viscosity, followed by gelation and conversion

to a solid elastomer. Pot life is defined as the time required for viscosity to double after Parts A and B (base and curing agent) are mixed. *Sylgard* 184 Silicone Elastomer has a pot life of >2 hours.

Processing and Curing

Thoroughly mixed *Sylgard* 184 Silicone Elastomer may be poured/dispensed directly into the container in which it is to be cured. Care should be taken to minimize air entrapment. When practical, pouring/dispensing should be done under vacuum, particularly if the component being potted or encapsulated has many small voids. If this technique cannot be used, the unit should be evacuated after the silicone encapsulant has been poured/dispensed.

Sylgard 184 Silicone Elastomer may be either room temperature (25°C/77°F) or heat cured following this schedule:

~48 hours at room temperature
45 minutes at 100°C (212°F)
20 minutes at 125°C (257°F)
10 minutes at 150°C (302°F)

These data are believed to be typical and should be used as initial estimates of cure times. Times will vary slightly from batch to batch and can be longer or shorter due to thermal mass of your parts and your heating ramp rate. Pretesting is recommended to confirm adequate cure for your application.

Sylgard 184 Silicone Elastomer can be placed in service immediately following the completion of the cure schedule. No post cure is required.

SURFACE PREPARATION

In applications requiring adhesion, priming is required. For best results, the primer should be applied in a very thin, uniform coating and then wiped off after application. The surface should be thoroughly air-dried prior to application of the silicone elastomer. Instructions for primer usage can be found in the Dow Corning literature, "How To Use *Dow Corning* Primers and Adhesion Promoters" (Form No. 10-366) and in the information sheets specific to the individual primers.

USEFUL TEMPERATURE RANGES

For most uses, *Sylgard* 184 Silicone Elastomer should be operational over a temperature range of -45 to 200°C (-49 to 392°F) for long periods of time. However, at both the low and high temperature ends of the spectrum, behavior of the materials and performance in particular applications can become more complex and require additional considerations.

For low-temperature performance, thermal cycling to conditions such as -55°C (-67°F) may be possible, but performance should be verified for your parts or assemblies. Factors that may influence performance are configuration and stress sensitivity of components, cooling rates and hold times, and prior temperature history.

At the high-temperature end, the durability of the cured silicone elastomer is time- and temperature-dependent. As expected, the higher the temperature, the shorter the time the material will remain usable.

COMPATIBILITY

Certain materials, chemicals, curing agents, and plasticizers can inhibit the cure of *Sylgard* 184 Silicone Elastomer. Most notable of these include:

- Organotin and other organometallic compounds
- Silicone rubber containing organotin catalyst
- Sulfur, polysulfides, polysulfones, or other sulfur-containing materials
- Amines, urethanes, or amine-containing materials
- Unsaturated hydrocarbon plasticizers
- Some solder flux residues

If a substrate or material is questionable with respect to potentially causing inhibition of cure, it is recommended that a small-scale compatibility test be run to ascertain suitability in a given application. The presence of liquid or uncured product at the interface between the questionable substrate and the cured gel indicates incompatibility and inhibition of cure.

HANDLING PRECAUTIONS

PRODUCT SAFETY INFORMATION REQUIRED FOR SAFE USE IS NOT INCLUDED IN THIS DOCUMENT. BEFORE HANDLING, READ PRODUCT AND MATERIAL SAFETY DATA SHEETS AND CONTAINER LABELS FOR SAFE USE, PHYSICAL, AND HEALTH HAZARD INFORMATION. THE MATERIAL SAFETY DATA SHEET IS AVAILABLE ON THE DOW CORNING WEBSITE AT WWW.DOWCORNING.COM, OR FROM YOUR DOW CORNING REPRESENTATIVE, OR DISTRIBUTOR, OR BY CALLING YOUR GLOBAL DOW CORNING CONNECTION.

USABLE LIFE AND STORAGE

Sylgard 184 Silicone Elastomer has a shelf life of 24 months from date of manufacture at room temperature.

For best results, *Sylgard* 184 Silicone Elastomer should be stored at or below 25°C (77°F). Special precautions must be taken to prevent moisture from contacting this material. Containers should be kept tightly closed and head or air space minimized. Partially filled containers should be purged with dry air or other gases, such as nitrogen.

PACKAGING

Sylgard 184 Silicone Elastomer is supplied in nominal 0.45-, 3.6-, 18- and 200-kg (1-, 8-, 40- and 440-lb) containers, net weight. Packaging options may vary.

Consult Dow Corning Customer Service at (989) 496-6000 for additional packaging options.

LIMITATIONS

This product is neither tested nor represented as suitable for medical or pharmaceutical uses.

HEALTH AND ENVIRONMENTAL INFORMATION

To support customers in their product safety needs, Dow Corning has an extensive Product Stewardship organ-

ization and a team of Product Safety and Regulatory Compliance (PS&RC) specialists available in each area.

For further information, please see our website, www.dowcorning.com, or consult your local Dow Corning representative.

**LIMITED WARRANTY
INFORMATION – PLEASE
READ CAREFULLY**

The information contained herein is offered in good faith and is believed to be accurate. However, because conditions and methods of use of our products are beyond our control, this

information should not be used in substitution for customer's tests to ensure that Dow Corning's products are safe, effective, and fully satisfactory for the intended end use. Suggestions of use shall not be taken as inducements to infringe any patent.

Dow Corning's sole warranty is that the product will meet the Dow Corning sales specifications in effect at the time of shipment.

Your exclusive remedy for breach of such warranty is limited to refund of purchase price or replacement of any

product shown to be other than as warranted.

**DOW CORNING SPECIFICALLY
DISCLAIMS ANY OTHER
EXPRESS OR IMPLIED WAR-
RANTY OF FITNESS FOR A
PARTICULAR PURPOSE OR
MERCHANTABILITY.**

**DOW CORNING DISCLAIMS
LIABILITY FOR ANY INCIDENT-
TAL OR CONSEQUENTIAL
DAMAGES.**

Appendix F: Drawing of Graphite Spring Electrode

